

Gravity Waves Signatures from Anisotropic pre-Inflation

A. E. Gümrükçüoğlu¹, L. Kofman² and M. Peloso¹

¹ *School of Physics and Astronomy,*

University of Minnesota, Minneapolis, MN 55455, USA and

² *CITA, University of Toronto, 60 St. George st., Toronto, ON M5S 3H8, Canada*

(Dated: October 29, 2018)

Abstract

We show that expanding or contracting Kasner universes are unstable due to the amplification of gravitational waves (GW). As an application of this general relativity effect, we consider a pre-inflationary anisotropic geometry characterized by a Kasner-like expansion, which is driven dynamically towards inflation by a scalar field. We investigate the evolution of linear metric fluctuations around this background, and calculate the amplification of the long-wavelength GW of a certain polarization during the anisotropic expansion (this effect is absent for another GW polarization, and for scalar fluctuations). These GW are superimposed to the usual tensor modes of quantum origin from inflation, and are potentially observable if the total number of inflationary e-folds exceeds the minimum required to homogenize the observable universe only by a small margin. Their contribution to the temperature anisotropy angular power spectrum decreases with the multipole ℓ as ℓ^{-p} , where p depends on the slope of the initial GW power-spectrum. Constraints on the long-wavelength GW can be translated into limits on the total duration of inflation and the initial GW amplitude. The instability of classical GW (and zero-vacuum fluctuations of gravitons) during Kasner-like expansion (or contraction) may have other interesting applications. In particular, if GW become non-linear, they can significantly alter the geometry before the onset of inflation.

I. INTRODUCTION: ANISOTROPIC PRE-INFLATION

The inflationary stage of the very early universe explains the dynamical origin of the observed isotropic and homogeneous FRW geometry. The patch of the FRW geometry covers the cosmological horizon and beyond if inflation lasted

$$N = 62 - \ln \left(\frac{10^{16} \text{GeV}}{V^{1/4}} \right) + \Delta, \quad (1)$$

e-folds or longer. Here V is the potential energy of the inflation, and Δ is a correction from the (p)reheating stage after inflation, which is not essential for our discussion. Chaotic inflationary models, associated with a large energy (\sim GUT scale) of $V^{1/4} \sim 10^{16} \text{GeV}$, predict a very large number of inflationary e-folds, $N \gg 62$. Long-lasting inflation erases all classical anisotropies and inhomogeneities of the pre-inflationary stage. However, scalar and tensor vacuum fluctuations during inflation lead to almost scale free post-inflationary scalar and tensor metric inhomogeneities around our smooth observable FRW patch.

In particular, the amplitude of the gravitational waves generated from the vacuum fluctuations during inflation is proportional to $V^{1/2}$, $h_k \simeq \frac{H}{2\pi M_p} \sim \frac{V^{1/2}}{M_p^2}$ (where M_p is the reduced Planck mass). There are significant efforts to measure the B -mode of $\Delta T/T$ polarizations, since this will provide a direct probe of the scale of inflation. The current 95% C.L. limits on r (ratio of the tensor to scalar amplitudes of cosmological fluctuations) $r \lesssim 0.43$ (WMAP-only) and $r \lesssim 0.2$ (WMAP plus acoustic baryon oscillation, plus supernovae) [1] shall be improved to $r \lesssim 0.1$ by the Planck mission [2], to $r \lesssim 0.05$ by the C $_{\ell}$ over [3], EBEX [4], and Spider [5] experiments (see [6] for the study of a mission that can improve over these limits). While these limits imply a detection in the case of high energy inflation, a number of other inflationary models, including many of the string theory constructions have lower energy, and therefore lead to GW of much smaller amplitude, which are virtually unobservable through B mode polarization ¹.

In anticipation of the null signal observation of the primordial GW from inflation, it is worth thinking about other implementations of this result for the theory of inflation, besides putting limits on the energy scale $V^{1/4}$. There are models of inflation (including many string theory inflationary models) where the total number of e-folds, N , does not

¹ Future gravitational waves astronomy may allow to probe r up to the level 10^{-6} with BBO [7] or ultimate DECIGO [8] direct detection experiments.

exceed the minimum (1) by a large number. If the extra number of e-folds ΔN beyond (1) is relatively small then pre-inflationary inhomogeneities of the geometry are not erased completely, and their residuals can be subject to observational constraints. In the context of this idea, in this paper we suggest an additional mechanism to have observable gravitational waves associated with inflation. These gravitational waves are very different from the GW generated from the vacuum fluctuations during inflation. Firstly, they are the residual tensor inhomogeneities from the pre-inflationary stage. Secondly, they can be of a classical, rather than quantum, origin. Thirdly, while their initial amplitude and spectrum are given by the initial conditions, they are significantly affected by the number of “extra” e-folds ΔN . Therefore, observational limits on gravity waves result in constraints on a combination of ΔN and of the initial amplitude.

The choice of the initial geometry of the universe before inflation is wide open. In principle, one may assume an arbitrary geometry with significant tensor inhomogeneities component, and much smaller scalar inhomogeneities. This choice is, however, very artificial. A much more comfortable choice of the pre-inflationary stage will be a generic anisotropic Kasner-like geometry with small inhomogeneities around it. The origin of the anisotropic universe with the scalar field can be treated with quantum cosmology, or can be embedded in the modern context of the tunneling in the string theory landscape. In fact, a Kasner-like (Bianchi I) space was a rather typical choice in previous papers on pre-inflationary geometry, see e.g. [9]. Most of the works on an anisotropic pre-inflationary stage aimed to investigate how the initial anisotropy is diluted by the dynamics of the scalar field towards inflation [10].

The formalism of linear fluctuations about an anisotropic geometry driven by a scalar field toward inflation was constructed only recently [11, 12, 13, 14]. Besides the technical aspects of calculations of cosmological fluctuations, there is a substantial conceptual difference between computations in the standard inflationary setting and in the anisotropic case. For an isotropic space undergoing inflationary expansion, all the modes have an oscillator-like time-dependence at sufficiently early times, when their frequency coincides with their momentum. One can therefore use quantum initial conditions for these modes. This is no longer the case for an expansion starting from an initial Kasner singularity. In this case, a range of modes, which can potentially be observed today (if ΔN is not too large), are not oscillating initially and therefore cannot be quantized on the initial time hyper-surface; as

a consequence, there is an issue in providing the initial conditions for such modes. For this reason we will adopt another perspective, namely, we will consider generic small classical inhomogeneities around the homogeneous background, as an approximation to the more generic anisotropic and inhomogeneous cosmological solution.

Equipped with this philosophy, we consider an anisotropic expanding universe filled up by the scalar field with a potential $V(\phi)$ which is typical for the string theory inflation. We add generic linear metric fluctuations about this geometry. The evolution of these fluctuations is by itself an interesting academic subject. However, it acquires a special significance in the context of the GW signals from inflation, because of a new effect that we report here of amplification of long-wavelength GW modes during the Kasner expansion. This growth terminates when a mode enters the “average” Hubble radius (the average of that for all the three spatial directions), or, for larger wavelength modes, when the background geometry changes from anisotropic Kasner to isotropic inflationary expansion. We perform explicit computations in the case of an isotropy of two spatial directions. In this case the computation becomes much more transparent and explicitly k dependent. Fluctuations for arbitrary a, b, c were considered in the formalism of [12, 14], where the k dependence is not explicit. We verified that our results agree with [12, 14] in the axisymmetric $b = c$ limit. We find that only one of the two GW polarizations undergoes significant amplification. Therefore, even if we assume for simplicity equi-partition of the amplitudes of the three inhomogeneous physical modes of the system (the scalar and the two GW polarization) at the initial time, the final spectra that will be frozen at large scales in the inflationary regime will be very different from each other, in strong contrast to what is obtained in the standard inflationary computations.

This result can have different consequences, that we explore in the present work. Suppose that the growing GW mode is still linear (but significantly exceeds other modes) when the space becomes isotropic. Then, we can have significant yet linear classical GW fluctuations at the beginning of inflation, say of amplitude $\lesssim \mathcal{O}(1)$. If the modes which correspond to the largest scales that we can presently observe left the horizon after the first ΔN e-folds of inflation, their amplitude decreased by the factor $e^{-\Delta N}$ in this period. If ΔN is relatively small, say $\sim \mathcal{O}(10)$ the freeze out amplitude of these GW modes would be $\sim \mathcal{O}(10^{-6})$. The angular spectrum of these GW will rapidly decrease as the multipole number ℓ grows, since smaller angular scales are affected by modes which spend more time inside the horizon

during the inflationary stage.

Suppose instead that the growing GW mode becomes non-linear before the onset of inflation. In this case the background geometry departs from the original onset.

Besides the phenomenological signatures, it is interesting to study the origin of the amplification of the GW mode. It turns out that the effect of GW amplification is related to the anisotropic Kasner stage of expansion. Therefore we will separately study GW in the pure expanding Kasner cosmology. For completeness, we also include the study of GW in a contracting Kasner universe, which is especially interesting due to the universality of anisotropic Kasner approach to singularity.

The plan of the paper is the following. In Section II we discuss the evolution of the anisotropic universe driven by the scalar field towards inflation. In Section III we briefly review the formalism of the linear fluctuations in the case of a scalar field in an anisotropic geometry, paying particular attention to the GW modes. In Section IV we compute the amplification of one of the two GW modes that takes place at large scales in the anisotropic era. In Section V we discuss instead the evolution of the other two physical modes of the system. In Section VI we study the evolution of the perturbations in a pure Kasner expanding or contracting Universe. In Section VII we return to the cosmological set-up, and we compute the contribution of the GW polarization amplified during the anisotropic stage to the CMB temperature anisotropies. In particular, by requiring that the power in the quadrupole does not exceed the observed one, we set some limits on the initial amplitude of the perturbations vs. the duration of the inflationary stage. In Section VIII we summarize the results and list some open questions following from the present study, which we plan to address in a future work.

II. BACKGROUND GEOMETRY

The anisotropic Bianchi-I geometry is described by

$$ds^2 = -dt^2 + a^2 dx^2 + b^2 dy^2 + c^2 dz^2 , \quad (2)$$

where $a(t), b(t), c(t)$ are the scale factors for each of the three spatial directions.

We consider a scalar field ϕ in this geometry. Many string theory inflationary models (for examples see [17, 18]) have a very flat inflationary potential which changes abruptly around

its minima. Therefore, to mimic this situation, we will use a simple inflaton potential

$$V = V_0 (1 - e^{-\phi/\phi_0})^2 , \quad (3)$$

which has quadratic form $V \sim \phi^2$ around the minimum, and is almost flat $V \approx V_0$ away from it. To obtain the correct amplitude of scalar metric perturbations from inflation, we set

$$\frac{\phi_0}{M_p} = 10^{-3} , \quad V_0^{1/4} = 10^{13} \text{GeV} . \quad (4)$$

The background dynamics is governed by the Einstein equations for the scale factors in the presence of the effective cosmological constant V_0 , plus a possible contribution from the kinetic energy of the scalar field. Quantum cosmology or tunneling models of the initial expansion favor a small scalar field velocity. Therefore we select the small velocity initial conditions $\dot{\phi}^2 \ll V_0$. In this case the generic solutions of the Einstein equations with cosmological constant for a, b, c are known analytically (see e.g. [14]) and can be cast as

$$\left(a(t), b(t), c(t) \right) = (a_{in}, b_{in}, c_{in}) \left[\sinh(3H_0 t) \right]^{1/3} \left[\tanh \left(\frac{3}{2} H_0 t \right) \right]^{p_i - 1/3} , \quad (5)$$

where p_i are the Kasner indices, $\sum_{i=1}^3 p_i = 1$, $\sum_{i=1}^3 p_i^2 = 1$, and H_0 is the characteristic time-scale of isotropization by the cosmological constant, $H_0^2 = \frac{V_0}{3M_p^2}$, while a_{in}, b_{in}, c_{in} are the normalizations of the three scale factors

For earlier times $t \ll 1/H_0$ the anisotropic regime is described by the vacuum Kasner solution

$$\left(a(t), b(t), c(t) \right) = (a_0, b_0, c_0) \cdot t^{p_i} , \quad (6)$$

which corresponds to an overall expansion of the universe (the average scale factor $(abc)^{1/3} = t^{1/3}$ is increasing), although only two directions are expanding (two positive p_i -s) while the third one is contracting (the remaining p_i is negative).

For later time $t \gg 1/H_0$ the universe is isotropic and expanding exponentially

$$\left(a(t), b(t), c(t) \right) = (a_0, b_0, c_0) \cdot e^{H_0 t} , \quad (7)$$

where the constant normalizations a_0, b_0, c_0 are typically chosen to be equal.

It is instructive to follow the evolution of the curvature in the model. The Ricci tensor is (almost) constant throughout the evolution up to the end of inflation

$$R_\nu^\mu = \frac{1}{4} \delta_\nu^\mu R , \quad R = 12H_0^2 \quad (8)$$

At earlier times the Weyl tensor – i.e. the anisotropic component of the curvature tensor – gives

$$C^2 \equiv C^{\mu\nu\rho\sigma} C_{\mu\nu\rho\sigma} = -\frac{16 p_1 p_2 p_3}{t^4} , \quad (9)$$

and, for $t \ll 1/H_0$, $\sqrt{C^2}$ is much bigger than the isotropic components (8). This is why initially the contribution from the effective cosmological constant is negligible, and the vacuum Kasner solution (6) is a good approximation. In contrast, at later times $t \gg 1/H_0$

$$C^{\mu\nu\rho\sigma} C_{\mu\nu\rho\sigma} \sim e^{-6H_0 t} , \quad (10)$$

and the anisotropic part of the curvature becomes exponentially subdominant relative to its isotropic part driven by the cosmological constant. This is an illustration of the isotropization of the cosmological expansion produced by the scalar field potential. The timescale for the isotropization is $t_{\text{iso}} \equiv 1/H_0$.

In the following Sections we will study the equations for the linear fluctuations around the background (2), (5). These equations become significantly simpler and more transparent for the particular choice of an axi-symmetric geometry e.g. when $c = b$, and the metric is

$$ds^2 = -dt^2 + a^2 dx^2 + b^2 (dy^2 + dz^2) . \quad (11)$$

While the effect we will discuss is generic, for simplicity we will adopt the simpler geometry (11) rather than the general Bianchi-I space (2). In this case, the early time solution is a Kasner background with indices $p_1 = -1/3, p_2 = p_3 = 2/3$ ². Also, it will be useful to define an “average” Hubble parameter H and difference h between the expansion rates in x and y (or z) directions as

$$H \equiv \frac{H_a + 2 H_b}{3} , \quad h \equiv \frac{H_a - H_b}{\sqrt{3}} , \quad H_a = \frac{\dot{a}}{a} , \quad H_b = \frac{\dot{b}}{b} \quad (12)$$

At earlier times $H_a \approx -\frac{1}{3t}, H_b \approx \frac{2}{3t}$, while, at late times, $H_a = H_b \approx H_0$. The equation for the homogeneous scalar field is

$$\ddot{\phi} + 3H\dot{\phi} + V_{,\phi} = 0 . \quad (13)$$

² There is another axisymmetric asymptotic Kasner solution, with indices $p_1 = 1, p_2 = p_3 = 0$. The solution is a very special one, since it is the only Bianchi-I model with cosmological constant that is regular at $t = 0$ (as can be easily checked by computing the curvature invariants; e.g. $C^2 = 12 H_0^4$ at $t = 0$). For $H_0 = 0$, this space is actually Minkowski space-time in an accelerated frame. Due to its special nature, we disregard this solution in the present study.

Since the value of H is very large initially, $H \approx \frac{1}{3t}$, the Hubble friction keeps the field (practically) frozen at $\phi = \phi_{in}$ during the anisotropic stage. For $t > t_{iso}$, the universe becomes isotropic, and it enters a stage of slow roll inflation until ϕ rolls to the minimum of its potential.

We also will use another form of the metric (11), with the conformal time η . There is ambiguity in the choice of η , related to possible different choices of the scale factors in its relation with the physical time. We will use the average scale factor

$$a_{av} \equiv (ab^2)^{1/3} , \quad (14)$$

and define η through

$$dt = (ab^2)^{1/3} d\eta , \quad (15)$$

which, at early times, gives $\eta \propto t^{2/3}$. In this variable, the line element (11) reads

$$ds^2 = (ab^2)^{2/3} \left[-d\eta^2 + \left(\frac{a}{b}\right)^{4/3} dx^2 + \left(\frac{b}{a}\right)^{2/3} (dy^2 + dz^2) \right] . \quad (16)$$

In the following, dot denotes derivative wrt. physical time t , and prime denotes derivative wrt conformal time. Moreover, we always denote by H_a and H_b the Hubble parameters with respect to physical time.

III. LINEAR FLUCTUATIONS

In the FRW universe with a scalar field there are three physical modes of linear fluctuations. Two of them are related to the two polarizations h_+ and h_\times of the gravitational waves, and one to the scalar curvature fluctuations v induced by the fluctuations of the scalar field $\delta\phi$. All three modes in the isotropic case are decoupled from each other. The formalism for the linear fluctuations on a FRW background has been extended to the Bianchi-I anisotropic geometry in [11, 12, 13, 14]. Again, there are three physical modes; however, in the general case of arbitrary a, b, c the modes are mixed, i.e. their effective frequencies in the bi-linear action $\delta^2 S$ are not diagonal, as it is the case in the isotropic limit.

In a special case of the axi-symmetric Bianchi I geometry (11) one of the three linear modes of fluctuations, namely, one of the gravity waves modes, is decoupled from the other two. This makes the analysis of fluctuations much more transparent than the general $a \neq b \neq c$ case. While the effects we will discuss, we believe, is common for arbitrary a, b, c ,

we will consider linear fluctuations around the geometry (11). The computation follows the formalism of [13], where the reader is referred for more details.

The most general metric perturbations around (11) can be written as

$$g_{\mu\nu} = \begin{pmatrix} -a_{\text{av}}^2 (1 + 2\Phi) & a_{\text{av}} a \partial_1 \chi & a_{\text{av}} b (B_{,i} + B_i) \\ & a^2 (1 - 2\Psi) & a b \partial_1 (\tilde{B}_{,i} + \tilde{B}_i) \\ & & b^2 [(1 - 2\Sigma) \delta_{ij} + 2 E_{,ij} + E_{(i,j)}] \end{pmatrix}. \quad (17)$$

where the indices $i, j = 2, 3$ span the $\{y, z\}$ coordinates of the isotropic 2d subspace. The above modes are divided into 2d scalars ($\Phi, \chi, B, \Psi, \tilde{B}, \Sigma, E$) and 2d vectors (B_i, \tilde{B}_i, E_i , subject to the transversality conditions $\partial_i B_i = \partial_i \tilde{B}_i = \partial_i E_i = 0$)³ according to how these modes transform under rotations in the isotropic subspace. The two sets of modes are decoupled from each other at the linearized level. In addition, there is the perturbation of the inflaton field $\varphi = \phi + \delta\phi$, which is also a 2d scalar.

The gauge choice

$$\delta g_{1i, 2ds} = \delta g_{ij} = 0, \quad (18)$$

corresponding to $\tilde{B} = \Sigma = E = E_i = 0$, completely fixes the freedom of coordinate reparametrizations. It is convenient to work with the Fourier decomposition of the linearized perturbations. We can therefore fix a comoving momentum \mathbf{k} , and study the evolutions of the modes having that momentum. Since modes with different momenta are not coupled at the linearized level, this computation is exhaustive as long as we can solve the problem for any arbitrary value of \mathbf{k} . More precisely, we denote by k_L the component of the momentum along the anisotropic x direction, and by k_T the component in the orthogonal $y-z$ plane. We denote by p_L and by p_T the corresponding components of the physical momentum. Finally, we denote by k and p the magnitudes of the comoving and physical momenta, respectively. Therefore, we have

$$k^2 = k_L^2 + k_T^2, \quad p^2 = p_L^2 + p_T^2 = \left(\frac{k_L}{a}\right)^2 + \left(\frac{k_T}{b}\right)^2 \quad (19)$$

To identify the physical modes, one has to compute the action of the system up to the second order in these linear perturbations. One finds that the modes Φ, χ, B , and B_i ,

³ Notice that transverse 2d vectors have one degree of freedom; contrary to the 3d case, there are no transverse and traceless 2d tensors.

corresponding to the $\delta g_{0\mu}$ metric perturbations, are nondynamical, and can be integrated out of the action. This amounts in expressing the nondynamical fields (through their equations of motion) in terms of the dynamical ones, and in inserting these expressions back into the quadratic action. For instance, for the nondynamical 2d vector mode one finds

$$B_i = \left(\frac{b}{a}\right)^{1/3} \frac{p_L^2}{p^2} \left(\frac{a}{b} \tilde{B}_i\right)' \quad (20)$$

The analogous expressions for the 2d nondynamical scalar modes can be found in [13].

In this way, one obtains an action in terms of the three remaining dynamical modes $\delta\phi$, Ψ , \tilde{B}_i . Once canonically normalized, these modes correspond to the three physical perturbations of the system. The canonical variables are

$$V \equiv a_{\text{av}} \left[\delta\phi + \frac{p_T^2 \dot{\phi}}{H_a p_T^2 + H_b (2p_L^2 + p_T^2)} \Psi \right], \quad H_+ \equiv \frac{\sqrt{2} a_{\text{av}} M_p p_T^2 H_b}{H_a p_T^2 + H_b (2p_L^2 + p_T^2)} \Psi \quad (21)$$

and

$$H_\times \equiv \frac{M_p p_L}{\sqrt{2} p} a_{\text{av}} \epsilon_{ij} p_i \tilde{B}_j \quad (22)$$

where ϵ_{ij} is anti-symmetric and $\epsilon_{12} = 1$ (we stress that H_\times encodes only one degree of freedom, since, due to the transversality condition of the 2d vector modes, $p_i \tilde{B}_i = 0$).

The dynamical equations for the modes H_+ and V are coupled to each other, while that of the H_\times mode is decoupled

$$H_\times'' + \omega_\times^2 H_\times = 0$$

$$\begin{pmatrix} V \\ H_+ \end{pmatrix}'' + \begin{pmatrix} \omega_{11}^2 & \omega_{12}^2 \\ \omega_{12}^2 & \omega_{22}^2 \end{pmatrix} \begin{pmatrix} V \\ H_+ \end{pmatrix} = 0. \quad (23)$$

The explicit expressions for the frequency matrix ω_{ij} , ($i, j = 1, 2$) are rather tedious and given in [13].

In the limit of isotropic background, $b \rightarrow a$, also the 2d scalars decouple, and the frequencies become

$$\omega_\times^2, \omega_{22}^2 \rightarrow k^2 - \frac{a''}{a}$$

$$\omega_{11}^2 \rightarrow k^2 - \frac{z''}{z}, \quad z \equiv \frac{a^2 \phi'}{a'}$$

$$\omega_{12}^2 \rightarrow 0 \quad (24)$$

Therefore, the mode V becomes the standard scalar mode variable [19], associated to the curvature perturbation, while the modes H_+ and H_\times are associated to the two polarizations

of the gravitational waves. Also notice that without the scalar field there are two physical modes which, due to the residual 2d isotropy, are decoupled.

IV. DECOUPLED TENSOR POLARIZATION

Since there are no vector sources, the 2d vector system describes a polarization of a gravitational wave obeying the “free field equations” $\delta R_{\mu\nu} = 0$ (which reproduce the equation (20) and the first of (23)). As we now show, this mode undergoes an amplification, which does not occur for the other two modes. This can be understood from considering the frequency of this mode

$$\frac{\omega_{\times}^2}{a_{\text{av}}^2} = p_L^2 + p_T^2 + \frac{H_a^2 - 14 H_a H_b - 5 H_b^2}{9} + \frac{\dot{\phi}^2}{2M_p^2} - (H_a - H_b)^2 \frac{p_T^2 (-2p_L^2 + p_T^2)}{p^4}. \quad (25)$$

In the isotropic case, for which ω_{\times}^2 is given by (24), each mode is deeply inside the horizon, $k/a \gg H$, at asymptotically early times. This is due to the fact that H is nearly constant, while k/a is exponentially large at early times. As a consequence, $\omega_{\times} \simeq k$ in the asymptotic past, and the mode oscillates with constant amplitude. In the present case instead

$$p_L \propto a^{-1} \propto \eta^{1/2} \approx t^{1/3}, \quad p_T \propto b^{-1} \propto \eta^{-1} \approx t^{-2/3}, \quad H_a, H_b \propto \eta^{-3/2} \approx t^{-1} \quad (26)$$

at early times ($\eta, t \rightarrow 0^+$). Namely, as we go backwards in time towards the initial singularity, the anisotropic direction becomes large, and the corresponding component of the momentum of the mode is redshifted to negligible values. On the contrary, the two isotropic directions become small, and the corresponding component of the momentum is blueshifted. However, the magnitude of the two Hubble parameters increases even faster. Therefore, provided we can go sufficiently close to the singularity, the early behavior of each mode is controlled by the negative term proportional to the Hubble parameters in eq. (25).

To be more precise, if we denote by a_0 and b_0 the values of the two scale factors at some reference time η_0 close to the singularity, we have

$$\omega_{\times}^2 = a_{\text{av}}^2(\eta) \left[-\frac{2}{a_{\text{av}}^2(\eta_0)} \frac{\eta_0}{\eta^3} + \frac{k_T^2}{b_0^2} \left(\frac{\eta_0}{\eta} \right)^2 + \mathcal{O}(\eta^0) \right] \quad (27)$$

where the first term in the expansion comes from the terms proportional to $H_{a,b}^2$ in eq. (25), while the second term from the component of the momentum in the isotropic plane (cf. the early time dependences with those given in eq. (26)). We see that the frequency squared

is negative close to the singularity, so that the mode H_\times experiences a growth⁴. In a pure Kasner geometry, the relations (26) hold at all times. Therefore, one would find $p_L \gg p_T \gg H_{a,b}$ at asymptotically late times. For brevity, we will loosely say that the mode “enters the two horizons $H_{a,b}^{-1}$ ” at late times; the meaning of this is simply that the frequency is controlled by the momentum in this regime, $\omega_\times^2 \simeq a_{\text{av}}^2 p^2 > 0$, and the mode H_\times enters in an oscillatory regime.

This simple description is affected by two considerations: firstly, we do not set the initial conditions for the modes arbitrarily close to the singularity, but at some fixed initial time η_0 ; Secondly, the geometry changes from (nearly) Kasner to (nearly) de Sitter due to the inflaton potential energy. Consequently, there are three types of modes of cosmological size. I: Modes with large momenta start inside the two horizons at η_0 . They oscillate ($\omega_\times^2 > 0$) all throughout the anisotropic regime, and they exit the horizon during the inflationary stage. II: Modes with intermediate momenta, for which (27) is a good approximation at η_0 . These modes enter the horizons, and start oscillating, at some time $\eta > \eta_0$ during the Kasner era; they exit the horizon later during inflation. III: Modes with small momenta, that are always outside the horizons, and never oscillate during the Kasner and inflationary regimes.

These considerations are crucial for the quantization of these modes. We can perform the quantization only as long as $\omega_\times^2 > 0$, and the mode is in the oscillatory regime. As we mentioned, during inflation, this is always the case in the past. Moreover, the frequency is adiabatically evolving ($\omega' \ll \omega^2$), and one can set quantum initial conditions for the mode in the adiabatic vacuum. This procedure is at the base of the theory of cosmological perturbations, and results in a nearly scale invariant spectrum at late times, once the modes have exited the horizon and become classical. In the case at hand, we cannot perform this procedure for modes of small momenta / large wavelength (modes III above). If inflation lasts sufficiently long, such modes are inflated to scales beyond the ones we can presently observe, so that the inability of providing initial quantum conditions is irrelevant for phenomenology. However, if inflation had a minimal duration, this problem potentially concerns the modes at the largest observable scales.

Irrespectively of the value of the frequency, it is natural to expect that the modes possess

⁴ A tachyonic frequency does not necessarily imply a growth of the physical fluctuations. For instance, this does not happen for the GW modes in the FRW geometry.

some “classical” initial value at η_0 . In the following we discuss the evolution of the perturbations starting with these initial conditions. Although we do not have a predictive way to set these initial values, we can at least attempt to constrain them from observations. In addition, we should worry whether the growth of H_\times can result in a departure from the Kasner regime beyond the perturbative level, in which case the background solution described in the previous Section may become invalid (we discuss this in Section VI).

As long as the frequency is accurately approximated by (27) in the Kasner regime, the evolution eq. for the mode H_\times is approximately solved by

$$H_\times = C_1 \sqrt{\eta} J_3 \left[2 k_T \left(\frac{a_0}{b_0} \right)^{1/3} \sqrt{\eta_0 \eta} \right] + C_2 \sqrt{\eta} Y_3 \left[2 k_T \left(\frac{a_0}{b_0} \right)^{1/3} \sqrt{\eta_0 \eta} \right] \quad (28)$$

where $C_{1,2}$ are two integration constants, while J and Y are the Bessel and Neumann functions. The first mode increases at early times (small argument in the Bessel function) $\propto \eta^2$, while the second one decreases as η^{-1} . We disregard the decreasing mode in the following computations, $C_2 = 0$ (moreover, this mode diverges at the singularity).

Rather than the time evolution of H_\times , we show in Figure 1 that of the corresponding power. We note the very different behavior obtained for large (III), intermediate (II), and small (I) scale modes. We choose to define the power spectrum as

$$P_{H_\times} \equiv \frac{a_{\text{av}}}{M_p^2 \pi^2} P^3 |H_\times|^2 \quad (29)$$

This definition coincides with the standard one (see for instance [20]) as the universe becomes isotropic. In particular, the power spectrum is frozen at large scales in the isotropic inflationary regime. Clearly, there is an ambiguity in this definition at early times, when the two scale factors differ (there is no a-priori reason for the choice of the average scale factor in this definition). This arbitrariness affects the time behavior shown in the Figure. However, it does not affect the relative behavior of the large vs. intermediate vs. small scale modes. Moreover, if we analogously define the power spectra for the 2d scalar modes, the relative behavior of these two types of mode (Figure 1 vs. Figure 4) is also unaffected by this arbitrary normalization.

The reality of this instability is demonstrated in Section VI, where we compute the squared Weyl invariant due to these fluctuations (more precisely, we do so in an exact Kasner background, which, as we have remarked, coincides with the cosmological background at asymptotically early times).

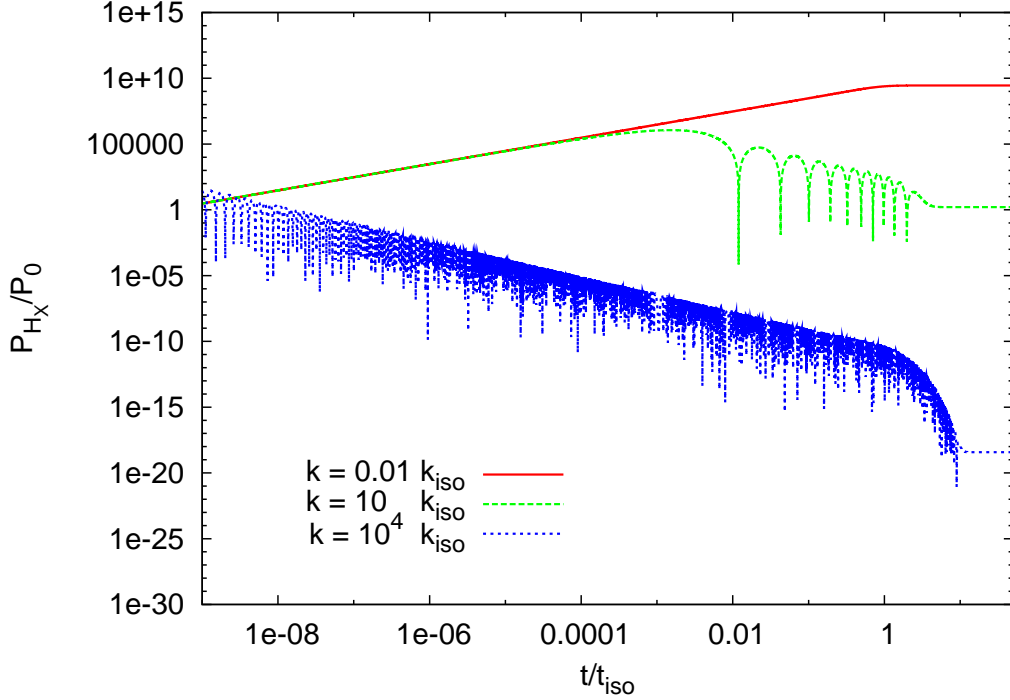


FIG. 1: Power in different modes of the decoupled tensor polarization, normalized to its initial value ($k_L = k_T$ for all the cases shown). We show the time evolution starting from $h_0 = -10^6 \sqrt{V_0}/M$ (defined in eq. 12). The universe isotropizes at $t_{\text{iso}} = 1/H_{\text{iso}}$. The quantity k_{iso} is defined to be the momentum of the modes exiting the horizon at this time. Large scale modes do not exhibit oscillatory behavior, and grow during the anisotropic stage. Intermediate scale modes enter the horizons during the anisotropic era; this terminates their growth. Small scale modes are in the oscillatory regime all throughout the anisotropic phase, and do not experience any growth. All modes shown freeze during the inflationary stage. Notice the very different final values obtained in the three cases shown.

In Figure 2 we show the power spectrum (normalized to the initial value for each mode) for the same background evolution as in the previous Figure, at some late time during inflation, when all the modes shown are frozen outside the horizon. As the approximate solution (28) indicates, the growth of H_\times occurs as long as the transverse momentum p_T is smaller than the Hubble rates $|H_{a,b}|$. Therefore, modes with smaller k_T experience a larger growth. We denote by θ the angle between the comoving momentum, and the anisotropic direction,

$$k_L = k \cos\theta \quad , \quad k_T = k \sin\theta \quad (30)$$

Therefore, in general, we expect a greater growth at smaller values of k (for any fixed θ) and at smaller values of θ (for any fixed k).⁵ This behavior is manifest in Figure 2. Modes with $k \ll k_{\text{iso}}$ experience the same growth during the Kasner era (since the leading expression for ω_\times^2 is independent of the momentum in this regime). Then, the modes shown in the Figure exhibit a very strong $\sim k^{-9}$ dependence for $k_{\text{iso}} \lesssim k \lesssim \text{few} \times 10^3 k_{\text{iso}}$. We also see an increase of the power as θ decreases. We stress that Figure 2 shows the contribution of each mode to the power spectrum normalized to the value that that contribution had at the initial time η_0 . Therefore, if the original spectrum has a scale, or an angular dependence, this will modify the final spectrum (for comparison, for the isotropic computation of modes with adiabatic quantum initial condition, $P_{H_\times} \propto k^3 |H_\times|^2 \propto k^2$ at early times).

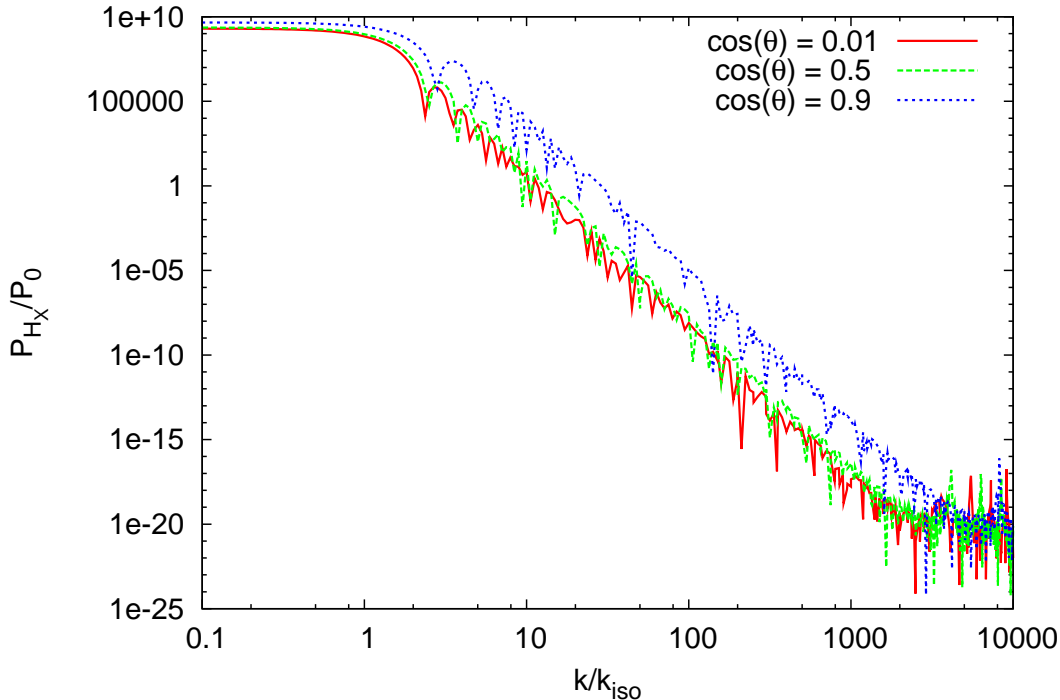


FIG. 2: Amplification of the power spectrum between the initial time (same as in the previous Figure) and some time during inflation for which the modes shown are outside the horizon, and the value of P_{H_\times} is frozen. As explained in the main text, the growth is greater at small values of k and θ .

The large growth at small θ is more manifest in Figure 3. The smallest angles shown in the Figure correspond to $k_T \ll k_L$, but to $p_T \gg p_L$ at the initial time (this is due to

⁵ Notice that, due to the planar symmetry of the background, the same results are obtained at θ and $\pi - \theta$.

the different behavior of the two scale factors in the anisotropic era). In this region, the spectrum exhibits a milder $P_{H_\times} \propto k^{-3}$ dependence than for intermediate values of θ . Finally, one may also consider smaller angles than those shown in the Figure, for which $p_T \leq p_L$ initially. We have found that final spectrum becomes θ -independent in this region.

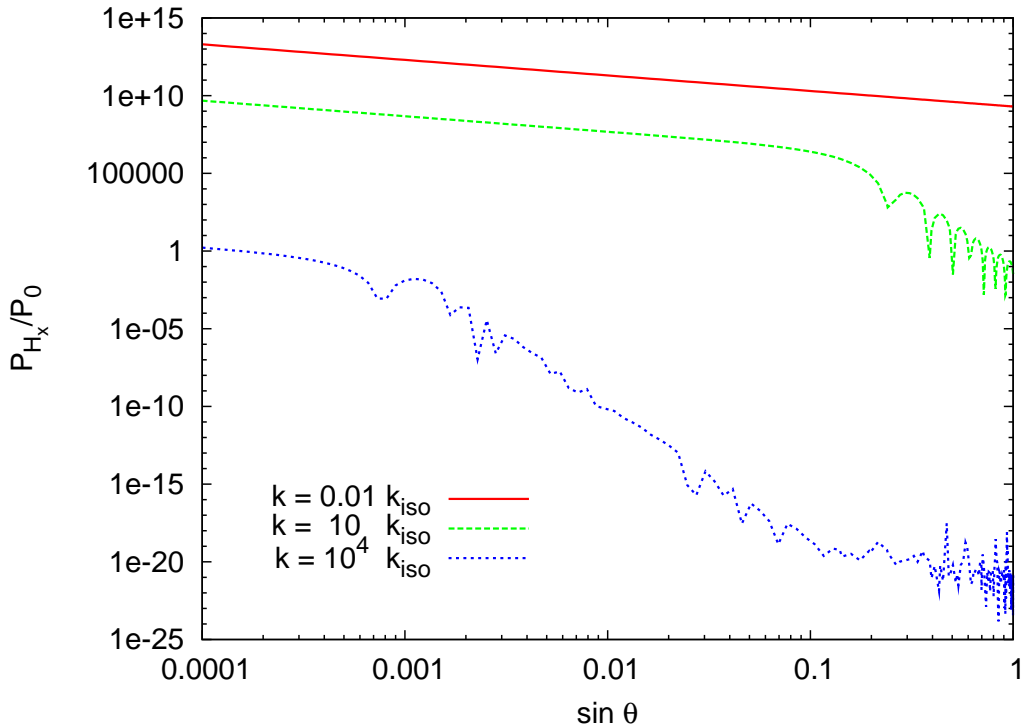


FIG. 3: Angular dependence of the power of different modes. We show the value reach by the mode once it is frozen in the inflationary stage, normalized to the initial value (the background evolution is identical to that of the previous two Figures). In the region $\theta \ll 1$ shown in the Figure ($k_T \ll k_L$) the final value exhibit a $1/\sin \theta$ dependence.

We conclude this section by discussing how the growth scales with the initial time. As long as $|H_{a,b}| \gg p_T \gg p_L$, the power (29) of a mode grows as $\eta^{3/2}$ (as can be easily seen by combining the time dependences $a_{av} \propto \eta^{1/2}$, $p \simeq p_T \propto \eta$, $H_\times \propto \eta^2$). We use the initial value of h (the difference between the two expansion rates, defined in eq. (12)) as a measure on the initial time, since, contrary to the conformal time, this quantity is not affected by the normalization of the scale factors. Starting with a greater value of $|h_0|$ corresponds to starting closer to the initial singularity, and, therefore, to a longer phase in which P_{H_\times} grows. Since $h \propto t^{-1} \propto \eta^{-3/2}$ in the Kasner regime, the ratio $P_{H_\times}/P_0 \propto |h_0|$ in the region in which the growth takes place. Although we do not show this here, we have verified that

this scaling is very well reproduced by the numerical results.

V. COUPLED TENSOR POLARIZATION-SCALAR MODE PAIR

As discussed in Section III the two other physical modes of the system are coupled to each other in the anisotropic era. The evolution equations for the coupled system are formally given in (23). At early times, we find

$$\begin{aligned}\omega_{11}^2, \omega_{22}^2 &= a_{\text{av}}^2(\eta) \left[\frac{1}{4 a_{\text{av}}^2(\eta_0)} \frac{\eta_0}{\eta^3} + \frac{k_T^2}{b_0^2} \left(\frac{\eta_0}{\eta} \right)^2 + \mathcal{O}(\eta^0) \right] \\ \omega_{12}^2 = \omega_{21}^2 &= a_{\text{av}}^2(\eta) \mathcal{O}(\eta^0)\end{aligned}\quad (31)$$

Therefore the coupling between the two modes can be neglected also at asymptotically early times. The main difference with the analogous expression for the decoupled tensor polarization, eq. (27), is that the squared eigenfrequencies of the two modes are now positive close to the singularity; therefore the two modes V , H_+ do not experience the same growth as H_\times . Indeed, as long as the expressions (31) are good approximations, we find the solution

$$H_+ = C_1^{H_+} \sqrt{\eta} J_0 \left[2 k_T \left(\frac{a_0}{b_0} \right)^{1/3} \sqrt{\eta_0 \eta} \right] + C_2^{H_+} \sqrt{\eta} Y_0 \left[2 k_T \left(\frac{a_0}{b_0} \right)^{1/3} \sqrt{\eta_0 \eta} \right] \quad (32)$$

and an identical one for V with the replacement $C_{1,2}^{H_+} \rightarrow C_{1,2}^V$ of the integration constants. Close to the singularity, the two modes grow as $\sqrt{\eta}$ and $\sqrt{\eta} \ln \eta$, respectively. Analogously to what we did for the H_\times polarization, we disregard the mode which grows less at early times, $C_2^{H_+} = C_2^V = 0$.

We define the power spectra for the tensor polarization, and for the comoving curvature perturbation R with the same prefactor as P_{H_\times} , cf. eq. (29),

$$P_{H_+} \equiv \frac{a_{\text{av}}}{\pi^2} p^3 |H_+|^2 \quad , \quad P_R \equiv \left(\frac{H}{\phi} \right)^2 \frac{a_{\text{av}}}{2\pi^2} p^3 |V|^2 \quad (33)$$

We see that, contrary to what happened for H_\times , the coupled perturbations, and the corresponding power spectra, do not grow while outside the horizons during the anisotropic era.

This effect is also manifest in Figure 5, where we show the spectra of the tensor mode H_+ and the comoving curvature for the same range of momenta, and for the same angles θ , as those of P_{H_\times} shown in Figure 2.

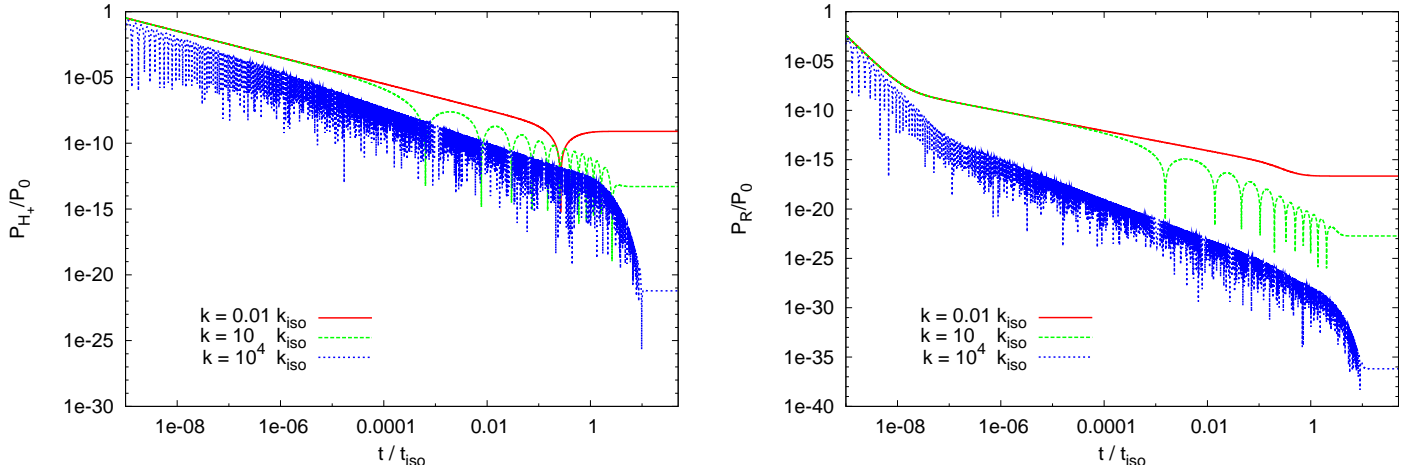


FIG. 4: Contribution of different modes to the power spectrum of the tensor polarization H_+ (left panel) and of the comoving curvature perturbation R (right panel), normalized to its initial value. The background evolution, and the momenta shown, are the same as in Figure 1. Contrary to the decoupled tensor mode, shown in Figure 1, the spectra do not grow while the modes are outside the horizons in the anisotropic regime.

VI. INSTABILITY OF KASNER SOLUTION AGAINST GRAVITATIONAL WAVES

The main result of the previous section was a significant amplification of the mode H_\times , compared to the milder amplification of the mode H_+ , in the anisotropic background which is undergoing isotropization due to the effect of a scalar field. This growth can be ascribed to the instability of the Kasner geometry, either contracting or expanding, against gravitational waves which we are going to report in this Section. Therefore in this Section we consider linearized gravity waves around an expanding and a contracting Kasner solution, without the presence of the scalar field, nor its fluctuation. In this case there are only the two decoupled modes H_\times and H_+ .

The claim of instability of the Kasner solution against the growth of the GW sounds at first glance heretic, at least for the contracting branch, in the light of the universality of the Belinskii-Khalatnikov-Lifshitz (BKL) oscillatory regime of the Kasner epochs approaching the singularity. In fact, it is not, and, on the contrary, it is compatible with the BKL analysis. Moreover, our finding of the GW instability suggests a new interpretation of the phenomena connected to the instability, discussed by BKL and others for the contracting

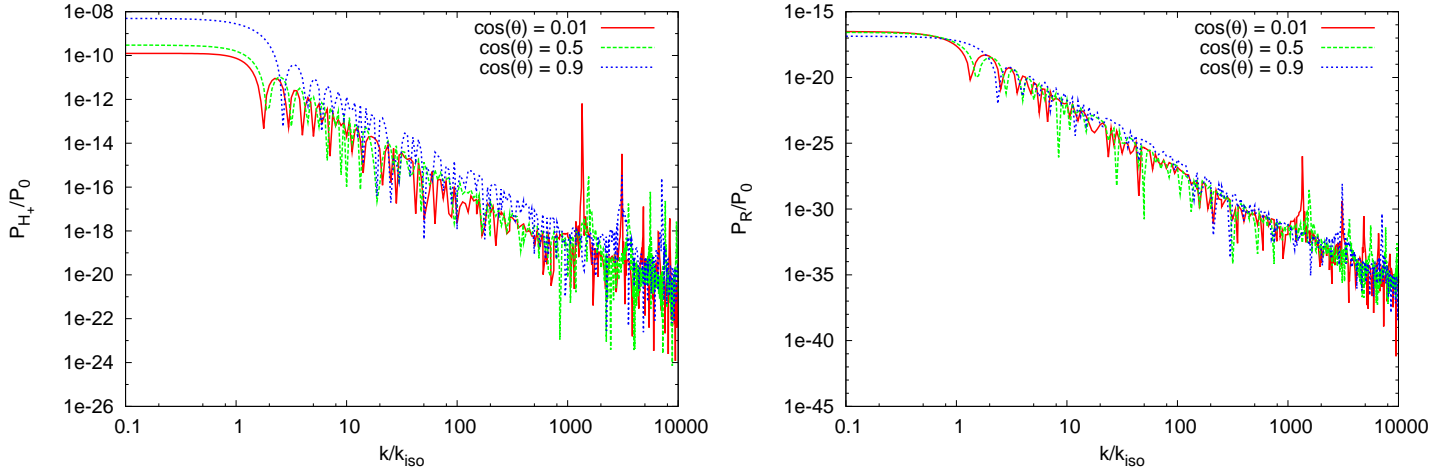


FIG. 5: Decrease of the power spectra of the tensor polarization H_+ (left panel) and of the comoving curvature R (right panel). The Figure shows the ratio between the power spectra at some time during inflation (when the modes are outside the horizon in the isotropic regime, and the spectra are frozen), and the initial time. The decrease should be compared with the growth experienced at large scales by P_{H_\times} , shown in Figure 2.

Kasner geometry in very different formalism and language [30, 31, 32, 33, 35].

In this Section we first perform linearized calculations for the classical gravitational waves around expanding and contracting Kasner solutions, and demonstrate their instabilities in terms of the evolution of the Weyl tensor invariant $C^{\mu\nu\rho\sigma}C_{\mu\nu\rho\sigma}$, which is independent of the gauge choice. We then connect the result with the BKL analysis.

The background line element is given by equation (16), with the scale factors

$$a = a_0 \left| \frac{\eta_0}{\eta} \right|^{1/2}, \quad b = b_0 \left| \frac{\eta}{\eta_0} \right| \quad (34)$$

This compact notation describes two disconnected geometries, at negative and positive conformal times, respectively. The algebraic expressions below simplify if we introduce the time η_* in which the normalization of the two scale factors coincide. Therefore, rather than (34), we can also use

$$a = a_* \left| \frac{\eta_*}{\eta} \right|^{1/2}, \quad b = a_* \left| \frac{\eta}{\eta_*} \right| \quad (35)$$

The two Hubble rates are

$$H_a = -\frac{1}{2a_*} \left| \frac{\eta_*}{\eta} \right|^{1/2} \frac{1}{\eta}, \quad H_b = \frac{1}{a_*} \left| \frac{\eta_*}{\eta} \right|^{1/2} \frac{1}{\eta} \quad (36)$$

while the average scale factor is $a_{\text{av}} = a_* \sqrt{\eta/\eta_*}$. The physical and conformal times are related by

$$dt = a_{\text{av}} d\eta \quad \Rightarrow \quad t = \frac{2 a_*}{3} \left| \frac{\eta}{\eta_*} \right|^{1/2} \eta \quad (37)$$

For future use, we also define t_* to be the physical time corresponding to η_* .

The solution with negative conformal time describes an overall contracting geometry, $a_{\text{av}} \propto (-\eta)^{1/2}$, which crunches into the singularity at $\eta = 0$. The solution with positive conformal time describes instead an overall expanding space, $a_{\text{av}} \propto \eta^{1/2}$, originating at the singularity at $\eta = 0$. As in the previous Sections, we restrict the computation to the simpler case of a residual 2d isotropy between two spatial directions. We expect that the instability occurs for general Kasner indices (p_1, p_2, p_3) .

Now we turn to the linearized perturbations satisfying the vacuum equations $\delta R_{\mu\nu} = 0$. There are two gravitational waves polarization perturbations. We consider a single mode with a given comoving momentum with components k_L and k_T . We denote by $\vec{\xi}$ the vector in the $y - z$ plane along the direction of \vec{k}_T ,

$$H(\eta, \vec{x}) = e^{-ik_L x - i\vec{k}_T \cdot \vec{\xi}} H(\eta, k_L, k_T) + \text{h.c.} \quad (38)$$

The two GW polarizations obey the equations

$$H''_{\times} + \omega_{\times}^2 H_{\times} = 0 \quad , \quad H''_{+} + \omega_{+}^2 H_{+} = 0 \quad , \quad (39)$$

where the effective frequencies can be written in compact form

$$\begin{aligned} \omega_{\times}^2 &= a_{\text{av}}^2 \left[p^2 + H_a^2 \frac{p_L^4 + 20p_L^2 p_T^2 - 8p_T^4}{p^4} \right] \quad , \\ \omega_{+}^2 &= a_{\text{av}}^2 \left[p^2 + H_a^2 \frac{16p_L^4 + 296p_L^2 p_T^2 + p_T^4}{(4p_L^2 + p_T^2)^2} \right] \quad , \end{aligned} \quad (40)$$

both for the contracting and the expanding backgrounds. We recall that the physical momenta are related to the comoving one by the relations (19).

After solving the two equations (39), we can compute the metric perturbations (17) and the Weyl tensor of the background plus perturbations. The square of the Weyl tensor, once expanded perturbatively, has the following schematic structure

$$C^{\mu\nu\rho\sigma} C_{\mu\nu\rho\sigma} = C^2 + C\delta C + \delta C^2 + \dots \quad , \quad (41)$$

where C^2 is the Weyl invariant for the non-perturbed background solution, $C\delta C$ is the term linear in H_{\times} and H_{+} , and δC^2 is the term quadratic in the perturbations. We do the

computation for the two polarizations separately. For instance, for the 2d vector modes, we compute the Weyl tensor in terms of the background and of the metric perturbations B_3 and \tilde{B}_3 . We then relate the two perturbations to H_\times through Eqs. (20) and (22), expressing spatial derivatives in terms of the comoving momenta, see Eq. (38). In this way, we can write the expression (41) in terms of H_\times , H_\times^* , and their time derivatives. Finally, we insert in this expression the solutions of Eq. (39). The procedure for the mode H_+ is analogous.

We compare the second and third term in (41) with the background term. A growth of the ratios $C \delta C / C^2$ (denoted as $\equiv \delta C / C$), or $\delta C^2 / C^2$, signals an instability of the Kasner geometry. The background (zeroth order) Weyl invariant is

$$C^2 = \frac{12}{a_*^4} \frac{\eta_*^2}{\eta^6} = \frac{64}{27 t^4}. \quad (42)$$

The first order term $C \delta C$ vanishes identically for the H_\times polarization. It is nonzero for H_+ , and it oscillates in space as $\exp \left[\pm i \left(k_L x + \vec{k}_T \cdot \vec{\xi} \right) \right]$. The second order term δC^2 for the Fourier modes H_\times or H_+ has a part which is constant in space, plus two parts that oscillate in space as $\exp \left[\pm 2i \left(k_L x + \vec{k}_T \cdot \vec{\xi} \right) \right]$. In the following, we disregard the oscillatory parts in δC^2 .

The solutions H_\times and H_+ are either monotonically evolving in time, or oscillating, with an envelope that is monotonically evolving in time. The oscillatory regime takes place when the mode has a wavelength shorter than the Hubble radii, $p > |H_a|, |H_b|$, and are absent in the opposite regime. Eqs. (26) show the time dependence of the momentum and of the Hubble rates for the expanding Kasner solution. We see that, if we consider a complete background evolution, any mode starts in the large wavelength regime, and then goes in the short wavelength regime. Therefore, we expect that a mode is in the non-oscillatory regime sufficiently close to the singularity, and in the oscillatory regime sufficiently far from it (this behavior is manifest in the time evolutions shown). The same is true for the contracting background solution (with the obvious difference that early and late times interchange).

The time dependence of the Weyl invariant (or of its amplitude, when the mode is oscillating) is summarized in Table 1. More specifically, we show the ratio between the terms proportional to the perturbations and the background one, both for the expanding and the contracting Kasner. In the expanding case, a mode evolves from the large scale to the short scale regime. The opposite happens in the contracting case. Notice the the short scale behaviors in the expanding and contracting cases coincide. The same is not true for the two

	$\delta C/C$ for H_+	$\delta C^2/C^2$ for H_+	$\delta C^2/C^2$ for H_\times	
EXPANDING ($0 < t < \infty$)	$\begin{cases} \text{const.} \\ \text{const.} \end{cases}$	$\begin{cases} \text{const.} \\ t^{16/3} \end{cases}$	$\begin{cases} t^2 \\ t^4 \end{cases}$	\leftarrow large scales \leftarrow short scales
CONTRACTING ($-\infty < t < 0$)	$\begin{cases} \text{const.} \\ \ln t \end{cases}$	$\begin{cases} t ^{16/3} \\ t ^{-2/3} \end{cases}$	$\begin{cases} t ^4 \\ t ^{-2} \end{cases}$	\leftarrow short scales \leftarrow large scales

TABLE I: Summary table for the time dependence of $\delta C/C$ and of the (non-oscillating in space) part of $\delta C^2/C^2$.

large scales behaviors. The reason is that, in the expanding case, we set to zero one of the two solutions of Eq. (39) that is decreasing at early times, and that would diverge at the initial singularity. The different behaviors are discussed in details in the next Subsection and in Appendix A.

A. Contribution of the H_\times mode to the Weyl invariant

In this Subsection, we compute the contribution of the H_\times to the square of the Weyl tensor, both for an expanding and a contracting Kasner geometry. The analogous computation for the mode H_+ can instead be found in Appendix A.

1. H_\times mode during expansion

Plugging (35) into (40), the frequency has the large scales (early times) and short scales (late times) expansions

$$\omega_\times^2 \simeq \begin{cases} -\frac{2}{\eta^2} + k_T^2 \frac{\eta_*}{\eta} & , \text{ large scales} \\ k_L^2 \left(\frac{\eta}{\eta_*}\right)^2 & , \text{ short scales} \end{cases} . \quad (43)$$

Consequently, we have the asymptotic solutions

$$H_\times \simeq \begin{cases} C_1 \sqrt{\eta} J_3(2 k_T \sqrt{\eta_* \eta}) & , \text{ large scales} \\ \frac{\bar{C}_1}{\sqrt{\eta}} e^{i \frac{k_L \eta^2}{2 \eta_*}} + \frac{\bar{C}_2}{\sqrt{\eta}} e^{-i \frac{k_L \eta^2}{2 \eta_*}} & , \text{ short scales} \end{cases} . \quad (44)$$

where $C_1, \bar{C}_1, \bar{C}_2$ are three integration constants. In the early time solution we have disregarded a decaying mode that would diverge at $\eta \rightarrow 0$, and where the expression in the

second line is the large argument asymptotic expansion of the parabolic cylinder functions

$$D_{-1/2} \left[\sqrt{2} e^{\pm i \pi/4}, \sqrt{\frac{k_L}{\eta_*}} \eta \right] \quad (45)$$

which are solutions of the evolution equation with the short scales expanded frequency (43).

An extended computation of the square of the Weyl tensor (performed as outlined after Eq. (41)) leads to $C \delta C = 0$; for the non-oscillatory part of the quadratic term in the fluctuations we find instead

$$\delta C^2 \simeq \begin{cases} \frac{2|C_1|^2 k_T^6 \eta_*^6}{3 M_p^2 a_*^6 \eta^3} & , \text{ large scales} \\ \left(\bar{C}_1 \bar{C}_2^* e^{\frac{i k_L \eta^2}{\eta_*}} + \text{h.c.} \right) \frac{32 k_L^4}{M_p^2 a_*^6 \eta_*} & , \text{ short scales} \end{cases} . \quad (46)$$

Since the background square Weyl $C^2 \propto \eta^{-6}$, this computation indicates that the ratio $\delta C^2/C^2$ increases as η^3 in the large scales regime, while it oscillates in the short scales regime, with an amplitude that increases as η^6 .

In the left panel of Figure 6 we present the full numerical evolution of $\delta C^2/C^2$ for three modes with different momenta. The behavior of the modes that we find here (pure Kasner geometry) should be compared with that discussed in the previous Sections, where the initial Kasner evolution was followed by an isotropic inflationary stage. In the evolutions shown in that case (for instance, Figs. 1 and 4) we had isotropization at the time t_{iso} , and we started with an initial time of about $10^{-9} t_{\text{iso}}$. In the present case, the geometry does not undergo isotropization. However, the two scale factors are normalized in such a way that they are equal to each other at the time t_* , cf. eqs. (35). Therefore, we also choose $t_0 = 10^{-9} t_*$ in the present case. Also in analogy to the modes shown in Figs. 1 and 4, we define k_* to be the comoving momentum of the modes which have parametrically the same size as the average horizon at the time t_* , namely $k_*/a_* = 1/(3t_*)$ (cf. the expressions (36)). Moreover, we choose $k_L = k_T$ as in those two Figures.

Figure 6 confirms that each mode evolves from the non oscillatory large scales regime to the oscillatory short scales regime (the transition occurs at later times for modes of smaller momenta / larger scales). The time dependence of $\delta C^2/C^2$ shown in the Figure agrees with the one obtained analytically, and summarized in Table I. For comparison we also plot in the Figure 6 the evolutions of the H_+ mode during expansion considered in the Appendix A(a).

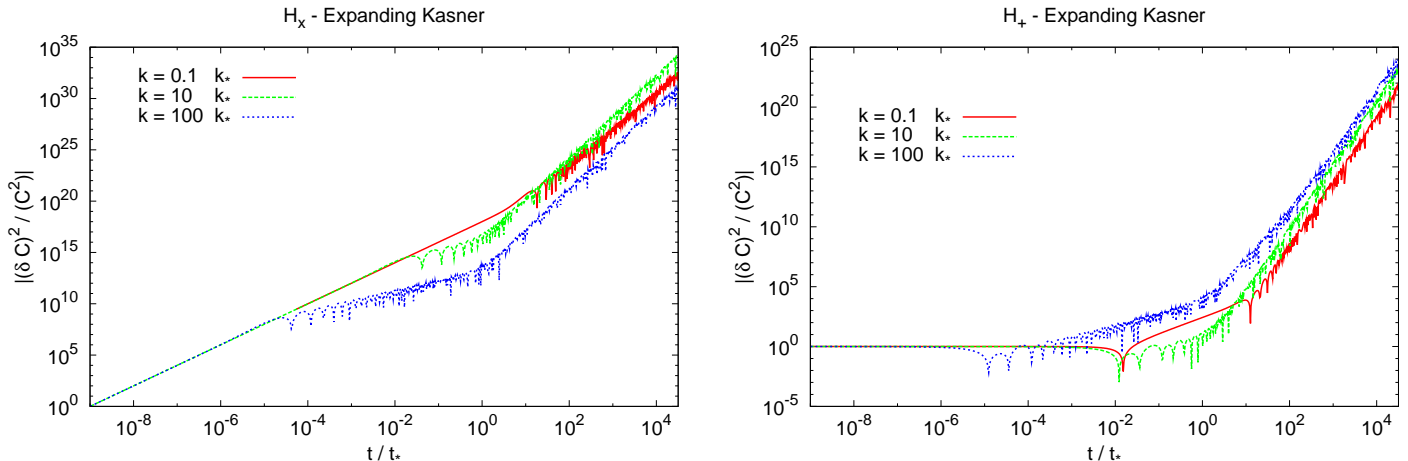


FIG. 6: Contribution to $\delta C^2/C^2$, defined in eq. (41), from H_\times (left panel) and H_+ (right panel) modes with some fixed comoving momentum. The time t_* is a reference time at which the two scale factors have the same normalization. k_* is the comoving momentum of the modes which have parametrically the same size as the two horizons at the time t_* ($k_L = k_T$ in all the cases shown). See the discussions after eqs. (46) and (A4) for more details.

The results shown in the Figure confirm the instability of the background Kasner solution against the GW polarization H_\times . The growth in the large scales regime (early times) agrees with the amplification of the power spectrum shown in Figure 1. However, contrary to what one would deduce from Figure 1, we see that the growth continues also in the short scales (late times) regime. We recall that the definition of the power spectrum (29) contains an arbitrariness in the overall time dependence (since one may have used a different combination of the two scale factors as overall normalization). We nonetheless adopted it to show the strong scale dependence of the evolution of the power spectrum (which is not affected by the overall normalization), and the very different evolution experienced by the two GW polarizations (which is also independent of the arbitrary normalization, since P_{H_\times} and P_{H_+} are normalized in the same way). To properly study the instability, one must study invariant and unambiguous quantities, such as the (scalar) square of the Weyl tensor which is investigated in this Section.

2. H_\times mode during contraction

We consider now the contribution to the square of the Weyl tensor from the mode H_\times in a contracting Kasner geometry. Plugging (35) into (40), the frequency of the H_\times mode on the contracting background has the short and large scales expansions

$$\omega_\times^2 \simeq \begin{cases} k_L^2 \left(\frac{-\eta}{-\eta_*} \right)^2 & , \text{ short scales} \\ -\frac{2}{(-\eta)^2} + k_T^2 \frac{-\eta_*}{-\eta} & , \text{ large scales} \end{cases} . \quad (47)$$

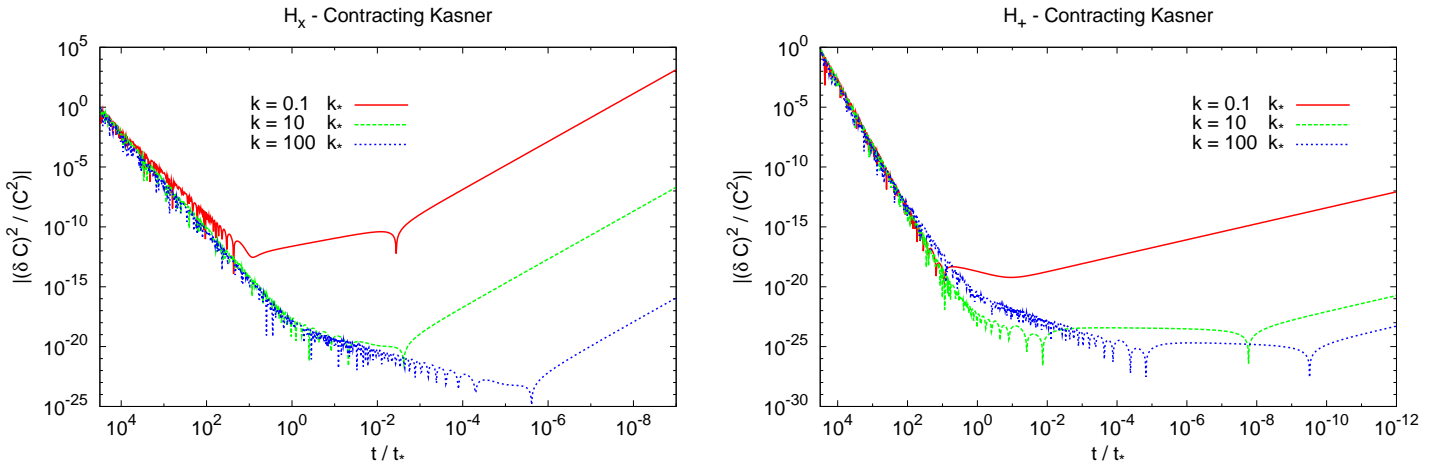


FIG. 7: Contribution to $\delta C^2/C^2$, defined in eq. (41), from H_\times (left panel) and H_+ (right panel) modes with some fixed comoving momentum. The times and momenta are chosen as in Figure 6. While in Figure 6 the background geometry is expanding (from the singularity at $t = 0^+$), the background geometry is contracting (towards the singularity at $t = 0^-$) in the evolutions shown here.

Once expressed in terms of absolute values of the time, the short and late time asymptotic expressions coincide with those of the expanding case, cf. eqs. (43). As in the expanding case, the short scales regime occurs asymptotically far from the singularity, while the large scales regime occurs asymptotically close to the singularity (notice, however, that a mode evolves from the large scales to the short scales regime in the expanding Kasner, while from the short scales to the large scales regime in the contracting Kasner background).

Consequently, also the short and large scales asymptotical solutions are identical, once

expressed in terms of η and η_* .

$$H_\times \simeq \begin{cases} \frac{C_1}{\sqrt{-\eta}} e^{i \frac{k_L (-\eta)^2}{2(-\eta_*)}} + \frac{C_2}{\sqrt{-\eta}} e^{-i \frac{k_L (-\eta)^2}{2(-\eta_*)}} & , \text{ short scales} \\ \bar{C}_1 \sqrt{-\eta} J_3 \left(2 k_T \sqrt{(-\eta_*) (-\eta)} \right) + \bar{C}_2 \sqrt{-\eta} Y_3 \left(2 k_T \sqrt{(-\eta_*) (-\eta)} \right) & , \text{ large scales} \end{cases} . \quad (48)$$

However, in contrast to the expanding case, we now keep both solutions for H_\times in the large scales regime ⁶.

For the non-oscillatory part of the Weyl tensor we find

$$\delta C^2 \simeq \begin{cases} \left(C_1 C_2^* e^{\frac{i k_L (-\eta)^2}{(-\eta_*)}} + \text{h.c.} \right) \frac{32 k_L^4}{M_p^2 a_*^6 (-\eta_*)} & , \text{ short scales} \\ \frac{480 |\bar{C}_2|^2}{M_p^2 \pi^2 a_*^6 k_T^6 (-\eta)^9} & , \text{ large scales} \end{cases} . \quad (49)$$

Notice that the short scales asymptotic evolution agrees with the corresponding one in the expanding case. However, in the large scale regime δC^2 is now controlled by the mode that was disregarded in the expanding background.

The asymptotic behaviors (49) are confirmed by the fully numerical evolutions shown in the left panel of Figure 7. For comparison we also plot the evolutions of the H_+ mode considered in the Appendix A(b).

B. Comparison with (in)stability analysis of BKL

How does the instability of gravitational waves which we demonstrated above fit with the classical picture of the universality of the rule of alternation of the Kasner epochs during contraction towards a singularity?

Let us briefly recall this picture. One of the points of the original paper [28] was to extend the anisotropic homogeneous contracting Kasner solution to a class of generalized Kasner solutions, describing more general inhomogeneous anisotropic geometries. It was implicitly assumed that there are large-scale, super-horizon inhomogeneities at the scales exceeding the (average) Hubble radius. Generic anisotropic solution shall contain eight physically different arbitrary functions of the spatial coordinates. However, it was identified by [28] that the homogeneous Kasner solution is unstable against a particular inhomogeneous mode

⁶ We recall that this mode was disregarded in the solution (44), since it is a decreasing mode in that case. In the contracting case instead this mode dominates at late times.

for which $\vec{l} \times \text{rot} \vec{l} = 0$ (here \vec{l} is the Kasner axes corresponding to the direction that is expanding). In other words, this mode is unstable and is growing with time. Therefore the monotonic (stable) inhomogeneous solution can have only seven arbitrary functions of the spatial coordinates. Homogeneous Kasner contraction (in Bianchi models with spatial curvature) occurs in the stochastic regime of alternation of Kasner exponents [29]. This influenced the philosophy of inhomogeneous generalization of the Kasner contraction. Following [30], now one can allow all eight arbitrary functions to describe generalized Kasner (Bianchi I) geometry. According to [30], the backreaction of the growing mode of the spatial instability alters the Kasner exponents of the patch of the contracting universe in the same manner as they were altered in the homogeneous Kasner-oscillating universe. Again, in this picture the inhomogeneity scale is larger than the “Hubble” patch, so that locally, along the time geodesics, the contraction is asymptotically homogeneous [33]. The instability induced by the spatial curvature associated with the inhomogeneous growing mode, and the resulting rotation of the Kasner axes were rigorously studied with the mathematical tools of the theory of dynamical systems in [34, 35].

In the previous Section we found instabilities of both expanding and contracting Kasner geometries against gravitational waves. Here for comparison with the BKL analysis we focus on the GW instability in the contracting universe. In this background, both polarizations H_\times and H_+ are unstable in the large wavelength limit. All physical wavelengths of the GW corresponding to the momenta k_1, k_2, k_3 in different directions (associated with different Kasner exponents) sooner or later will leave the Hubble radius $\sim 1/H \sim t$, independently of whether they are red- or blue-shifted. The physical frequency of the two modes has the structure $\omega^2 \sim \frac{k_1^2}{a^2} + \frac{k_2^2}{b^2} + \frac{k_3^2}{c^2} + f(H_a, H_b)$, where the function f is of order of $H_{a,b}^2$. For small t this function dominates over the momenta terms; this turns the time dependence of the GW amplitude from the oscillating to the non-oscillating regime. The amplitude of the non-oscillating GW increases with time in this long-wavelength regime, signaling the instability which we described in the previous Section. It turns out (See Appendix B) that these unstable GW modes in the long-wavelength limit exactly coincide with the unstable solution $\vec{l} \times \text{rot} \vec{l} = 0$ found in [28]. Phrased in another way, the unstable solution of [28] which destroys the monotonicity of the homogeneous Kasner contraction is nothing but the GW polarizations that are evolving with time into the long-wavelength regime. This provides us with a new insight into the origin of the generalized inhomogeneous contracting

Kasner solution: small short-wavelength GW will eventually be stretched to become the long-wavelength inhomogeneous modes, which are unstable.

Equipped with the BKL conjecture, one may think that for the contracting universe the growth of the unstable GW modes results in an alternation of the Kasner exponents. While this conjecture is supported for a contracting universe [21, 30], it is not clear how the GW instability evolves for the expanding Kasner background. Indeed, for contracting Kasner universe GW leave the Hubble radius and become long-wavelength inhomogeneities, and their backreaction can be described by the impact of the spatial curvature at the “local” time evolution of $a(t), b(t), c(t)$. For an expanding universe, initially long-wavelength GW enter the Hubble radius. Their backreaction can be treated with the pseudo-tensor $T_{\mu\nu} = M_p^2 \langle h_{;\mu}^{\rho\sigma} h_{\rho\sigma;\nu} \rangle$ for the high-frequency GW.

Another interesting issue is how our unstable modes correspond to the perturbatively small variations of the Kasner exponents (giving contribution to the diagonal metric fluctuations) as well as small variations of the Kasner axes (contribution to off-diagonal metric fluctuations).

Finally, one of the most interesting application of the effect is related to zero vacuum fluctuations of gravitons in contracting Kasner geometry, which are unstable. They grow and become large scale classical GW inhomogeneities described by the random gaussian field. One may think that the Kasner axes will be altered and rotated differently in different spatial domains of that random field.

We will expand these considerations in a forthcoming investigation.

VII. $\Delta T/T$ DUE TO THE RESIDUAL CLASSICAL GW FROM PRE-INFLATION

The growth of the decoupled tensor polarization at large scales can leave an imprint in the amplitude and in the polarization of the CMB anisotropies. A characteristic signature is a non-diagonal correlation between different multipoles in the expansion of the anisotropies, due to initial background anisotropy. Such extended phenomenological study is beyond the goals of the present work. However, we want to obtain a crude estimate on the limits that such a study would impose on the model, namely on the physical wavelength beyond which the statistics of the modes is anisotropic, and on the initial amplitude of the GW signal. For this reason, we compute the contribution of the GW mode to the quadrupole

of the temperature anisotropies, and we impose that it does not exceed the WMAP value $C_2 \simeq 3 \cdot 10^{-11}$ [24].

As we show in appendix C, the C_ℓ coefficients of the temperature anisotropies are related to the primordial spectrum of the GW by

$$C_\ell = \frac{9 \pi^3}{8} \frac{(\ell + 2)!}{(\ell - 2)!} \int_0^\infty \frac{d(k \eta_0)}{(k \eta_0)} I_\ell^2(k \eta_0) \int_{-1}^{+1} \frac{d\xi}{2} \int_0^{2\pi} \frac{d\phi_k}{2\pi} [P_{H_+}(\mathbf{k}) + P_{H_\times}(\mathbf{k})] , \quad (50)$$

where I_ℓ is a “window function”, which for a matter dominated universe ⁷ is given in Eq. (C12). The analytic expression for $I_2(k \eta_0)$ can be found in [25]. In this case, the function peaks at $k \eta_0 \simeq 3$, while it goes to zero as $\sim (k \eta_0)^2$ at small argument, and as $\sim \cos(k \eta_0) / (k \eta_0)^2$ at large argument. The quantity η_0 is the present conformal time. For a matter dominated universe

$$H = \frac{2}{a_0 \eta} \Rightarrow \eta_0 = \frac{2}{a_0 H_0} \quad (51)$$

where here a_0 denotes the present value of the scale factor. The comoving momentum k of a mode is related to its present wavelength λ by $\lambda = 2 \pi / (k/a_0)$. Therefore the quantity

$$k \eta_0 = 2 \pi \left(\frac{2 H_0^{-1}}{\lambda} \right) \quad (52)$$

gives the present ratio between the size of the (particle) horizon and of the mode with comoving momentum k . As shown in Figure 2, the power spectrum of the decoupled tensor polarization experiences a growth only for $k < k_{\text{iso}}$. If the anisotropic stage is followed by a prolonged inflationary stage, these large scale modes are inflated to scales much larger than the present horizon size, $k_{\text{iso}} \eta_0 \propto H_0^{-1} / \lambda_{\text{iso}} \ll 1$, and the window function I_ℓ suppresses the contributions of these modes to the C_ℓ coefficients.

We now relate $k_{\text{iso}} \eta_0$ to the duration of inflation through the number of e-folds $N(k)$ between the moment in which the mode with comoving momentum k leaves the horizon during inflation, and the end of inflation. This quantity is [22]

$$N(k) = 62 - \ln \left(\frac{k}{a_0 H_0} \right) - \ln \left(\frac{10^{16} \text{GeV}}{V_0^{1/4}} \right) + \Delta , \quad (53)$$

⁷ With this assumption we disregard the modes that reentered the horizon during the radiation stage, which do not contribute significantly to lowest C_ℓ 's, and the period of late accelerated expansion; this is consistent with the present approximate computation.

For a matter dominated universe $a_0 H_0 = 2/\eta_0$, cf. eq. (51); V_0 is the energy density in the universe at the moment in which that mode left the horizon (for the potential we are discussing, cf. Eq. (3), this quantity is nearly independent of k); finally, the quantity Δ is sensitive to the details of reheating (see [23] for a discussion). Imposing that all the modes within the horizon today were sub-horizon at the beginning of inflation gives the minimal number of e-folds given in Eq. (1). We define

$$\Delta N \equiv N(k_{\text{iso}}) - N_{\text{min}} = -\ln\left(\frac{k_{\text{iso}}}{a_0 H_0}\right) = -\ln\left(\frac{k_{\text{iso}} \eta_0}{2}\right) \quad (54)$$

Since k_{iso} is the comoving momentum of the modes leaving the horizon when the universe becomes isotropic, ΔN is the difference in e-folds between the duration of the isotropic inflationary stage and the minimal duration (1). As we discussed, a large ΔN results in a suppressed effect of the amplified GW modes on the observed CMB anisotropies.

We compute only the contribution of H_\times to the C_2 coefficient in Eq. (50). Figures 2 and 3 give the power spectrum of this mode at the end of inflation normalized by the initial power spectrum P_0 . This quantity is related to the initial condition at the start of the anisotropic stage, and it was left unspecified. For definiteness, we parametrize it with an overall amplitude and with a power law dependence on the scale

$$P_0 = \mathcal{A}_0 \times (\eta_0 k)^n, \quad (55)$$

where \mathcal{A}_0 is the initial power at a scale which parametrically corresponds to the present horizon size. We numerically perform the angular integral in (50), to find

$$\bar{P}\left(\frac{k}{k_{\text{iso}}}\right) \equiv \int_{-1}^1 d\xi P_\times(k, \xi) \simeq 2 \times 10^3 \frac{|h_0|}{\sqrt{V_0}/\phi_0} \mathcal{A}_0 (\eta_0 k)^n \times \begin{cases} 1 & , k \lesssim k_{\text{iso}} \\ \left(\frac{k_{\text{iso}}}{k}\right)^3 & , k \gtrsim k_{\text{iso}} \end{cases} \quad (56)$$

where the proportionality to $|h_0|$ is related to the growth of the power spectrum during the anisotropic era, as explained at the end of Section IV. The dependence on k is due to the fact that the angular integral is dominated by modes of small angle ($k_L \gg k_T$), cf. Figure 3, where the growth of the spectrum is flat for $k \lesssim k_{\text{iso}}$, and scales as $\sim k^{-3}$ at larger k .

The function \bar{P} is shown in Figure 8, normalized by $|h_0|$ and by the initial power spectrum P_0 . The dependences on $|h_0|$ and on k given in eq. (56) are manifest in the Figure.

We can now perform the final integral over momenta in (50). Taking into account the large and small argument dependence of I_2 and that of \bar{P} given in eq. (56), we see that the

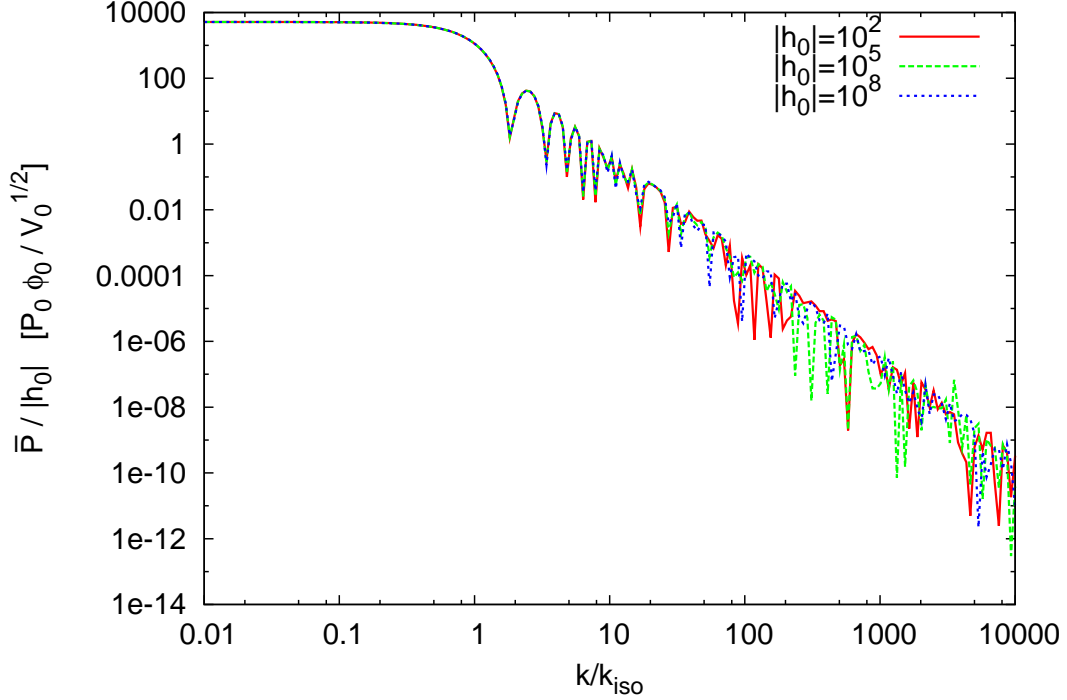


FIG. 8: Angular integral of the power spectrum, defined in Eq. (56). We show the result normalized by the initial power spectrum, starting from different values of $|h_0|$ (given in units of $\sqrt{V_0}/\phi_0$; larger values of this quantity corresponds to a longer anisotropic stage), and rescaling it by $|h_0|$, to explicitly show the linear dependence of the power spectrum on this quantity.

integrand behaves as $\sim k^{n-3}$ at small k , and as $\sim k^{n-8}$ at large k . Therefore, the integral converges for a wide range for the initial slope defined in Eq. (55), namely $-4 < n < 7$.

After performing the integral, we impose that the resulting C_2 does not exceed the WMAP value $C_2 \simeq 3 \cdot 10^{-11}$ [24]. This results in an upper limit on $\mathcal{A}_0 |h_0|$ (the initial overall amplitude, times the growth during the anisotropic phase) for any value of k_{iso} and n . We show this in Figure 9. As explained after Eq. (52), the limit weakens at small values of $k_{\text{iso}} \eta_0$, corresponding to a longer duration of the inflationary stage.

Finally, we show in Figure 10 the first few C_ℓ 's, normalized by the initial amplitude of the GW and the length of the anisotropic era (controlled by $|h_0|$), for a few values of the slope (55). As expected, for moderate slopes, the spectrum of C_ℓ decreases with ℓ . This is due to the fact that larger angular scales (small ℓ) are affected by the modes with lower momenta, which grow more during the anisotropic stage. The three spectra shown in the

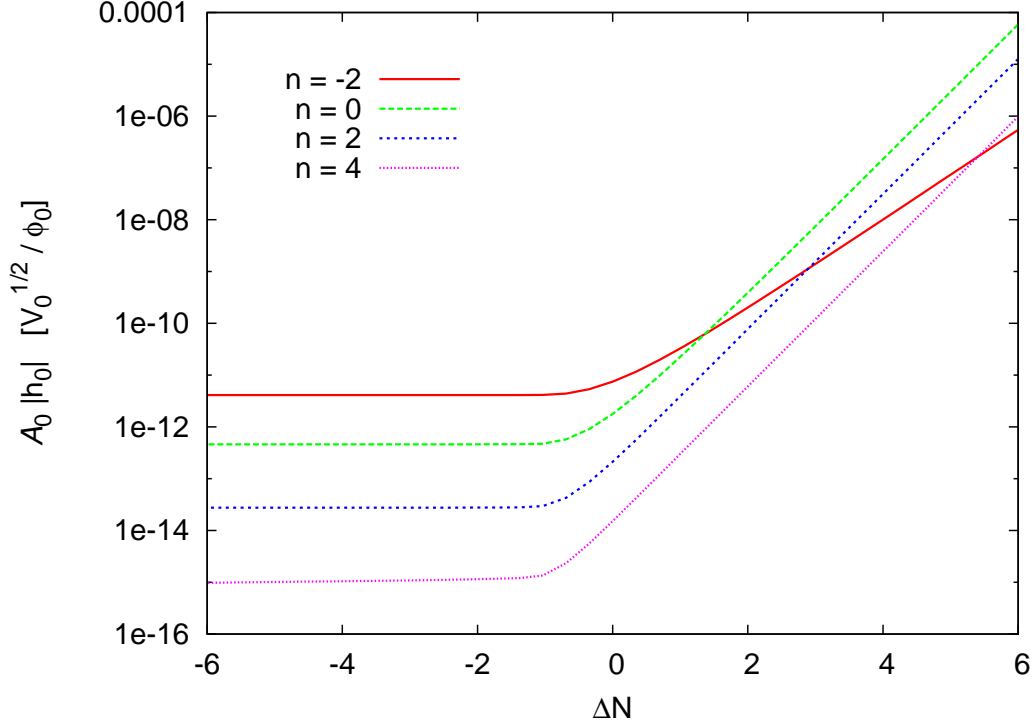


FIG. 9: Limit on the initial amplitude of the power spectrum, times its growth during the anisotropic stage. The quantity ΔN , defined in eq. (54), is the number of e-folds of isotropic inflation minus the minimum usually required to homogenize the universe, cf. eq. (1). For a longer duration of the inflationary stage, the modes experiencing the growth are inflated to larger scales than the present horizon, and the resulting effect is suppressed (weaker limit). \mathcal{A}_0 and n , are, respectively, the amplitude and the slope of the initial power spectrum, see eq. (55), while $|h_0|$ is proportional to the duration of the anisotropic stage.

figure can be fitted by a single power-law (with an accuracy up to about 10%):

$$C_\ell \simeq \begin{cases} 80 \ell^{-3.8} & , \quad n = -2 \\ 248 \ell^{-1.9} & , \quad n = 0 \\ 1430 \ell^{-0.4} & , \quad n = 2 \end{cases} \quad (57)$$

We see that the angular spectrum roughly decreases with ℓ as $C_\ell \sim 1/\ell^p$, where the exponent p depends on the power-spectrum of the classical GW at the initial hypersurface.

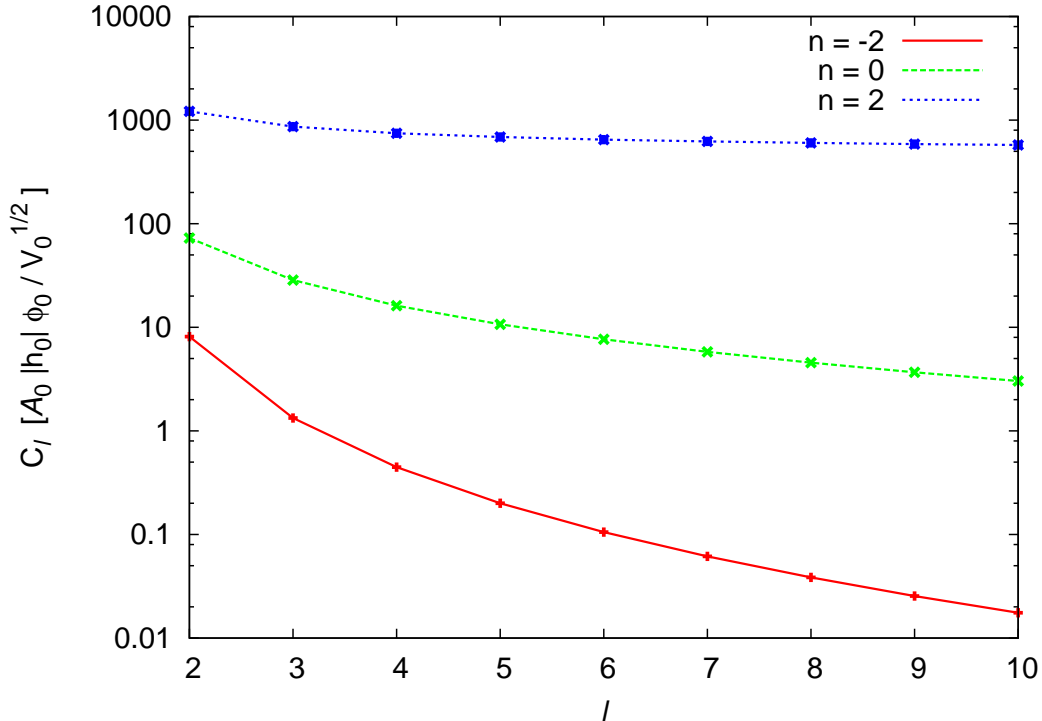


FIG. 10: First C_ℓ coefficients generated by the GW, normalized by the initial amplitude and the duration of the anisotropic era (controlled by $|h_0|$). The three curves correspond to three different slopes of the initial power in the GW, eq. (55).

VIII. DISCUSSION

We found a new effect of instability of the gravitational waves in an expanding and contracting Kasner geometries. We demonstrated the effect for a particular choice of the Kasner exponents $(-1/3, 2/3, 2/3)$, but we expect it is rather generic. This particular choice allows to simplify the description of GW in such a way that their wave equations are manifestly depending on the momenta. For the contracting Kasner geometry, we found that our unstable GW mode is identical to the unstable large-scale inhomogeneous mode first identified in [28]-[30] (for arbitrary Kasner exponents (p_1, p_2, p_3)). Backreaction of this unstable mode is conjectured to alter the Kasner exponents, differently in different spatial patches, depending on the spatial profile of the initial GW.

The Kasner geometry is a rather universal asymptotic solution for many interesting situations: it describes approach towards black holes or cosmological singularities (including higher dimensional and supersymmetric cases [36]), and it describes generic anisotropic expansion from singularity prior to inflation.

All of these situations are inevitably accompanied by quantum fluctuations of the gravitons), and, possibly, also by classical gravitational waves. There is a long list of questions arising in connection with a new effect of the gravity waves instability in anisotropic geometry. We have to investigate how the instability growth depends on the Kasner exponents p_1, p_2, p_3 . It will be interesting to understand if the instability of the classical GW also results in the instability of the graviton zero vacuum fluctuations. It will also be worth to understand the impact of the GW instability on the structure of the singularity inside the black hole and cosmological singularity. It is also interesting to investigate the backreaction of the GW instability on the contracting and expanding anisotropic geometries depending on the initial GW profile.

In this paper we considered the effect of GW instability in the context of the anisotropic pre-inflationary stage. The transition from Kasner expansion to inflation terminates the effect of GW instability but leaves classical GW signal as the initial conditions for inflation. If inflation does not last very long, then the residual GW can contribute to the CMB temperature anisotropies. Since GW polarizations and the scalar mode of cosmological fluctuations behave differently during anisotropic pre-inflation, we can consider only the leading contribution, namely, H_\times mode of the GW polarization. In this paper we calculated its contribution to the total $\Delta T/T$ anisotropy angular power spectrum. The angular power spectrum of the signal decreases with ℓ in a power-law manner and depends on the initial spectrum of the classical GW fluctuations, $C_\ell \sim 1/\ell^p$, where the exponent p depends on the power-spectrum of the classical GW at the initial hypersurface. It is interesting to note that this result is qualitatively similar to the result of [37], where the impact of GW from the our-universe-bubble nucleation was considered.

The signal from H_\times is rather anisotropic, and there is an interesting question about the anisotropy of its multipole structure $\langle a_{\ell m} a_{\ell' m'}^* \rangle$, which is intriguing in connection with an apparent alignment of the low multipoles of $\Delta T/T$. While such an analysis is beyond the aims of the present work, we have estimated the initial conditions (initial amplitude of the GW, versus the duration of inflation) which can lead to potentially observable effects. We leave a more extended analysis to future investigation.

Acknowledgements

We thank J.R. Bond, C.R. Contaldi, T. Damour, I. Khalatnikov, A. Linde, C. Pitrou, M. Sasaki, A. Starobinsky, J.P. Uzan and J. Weinwright for useful discussions and correspondence. The work of A.E.G. and M.P. was partially supported by the DOE grant DE-FG02-94ER-40823. LK was supported by NSERC and CIFAR.

APPENDIX A: CONTRIBUTION OF THE H_+ MODE TO THE WEYL INVARIANT

In this Appendix we compute the contribution of the H_+ mode to the square of the Weyl tensor for a pure Kasner background. We treat the expanding and contracting cases separately. This presentation follows the analogous one for the H_\times mode placed in Subsection VIA of the main text.

a. H_+ mode during expansion

Substituting (35) into (40) we have the large and short scale expansions

$$\omega_+^2 \simeq \begin{cases} \frac{1}{4\eta^2} + k_T^2 \frac{\eta_*}{\eta} & , \text{ large scales} \\ k_L^2 \left(\frac{\eta}{\eta_*}\right)^2 & , \text{ short scales} \end{cases} . \quad (\text{A1})$$

Consequently, we have the asymptotic solutions

$$H_+ \simeq \begin{cases} C_1 \sqrt{\eta} J_0(2k_T \sqrt{\eta_* \eta}) & , \text{ large scales} \\ \frac{\bar{C}_1}{\sqrt{\eta}} e^{i\frac{k_L \eta^2}{2\eta_*}} + \frac{\bar{C}_2}{\sqrt{\eta}} e^{-i\frac{k_L \eta^2}{2\eta_*}} & , \text{ short scales} \end{cases} . \quad (\text{A2})$$

where again in the early time solution we have disregarded a decaying mode that would diverge at the initial singularity. Notice that the late time expression is the same as for the H_\times mode (since the late time expansions of ω_\times^2 and ω_+^2 coincide).

For the linear part of the Weyl tensor we find

$$C \delta C \simeq e^{-ik_L x - ik_T y} \times \left\{ \begin{array}{l} \frac{-36\sqrt{2}C_1\eta_*^{5/2}}{M_p a_*^5 \eta^6} & , \text{ large scales} \\ \left(\bar{C}_1 e^{i\frac{k_L \eta^2}{2\eta_*}} + \bar{C}_2 e^{-i\frac{k_L \eta^2}{2\eta_*}} \right) \frac{12\sqrt{2}k_T^2 \eta_*^{7/2}}{M_p a_*^5 \eta^6} & , \text{ short scales} \end{array} \right\} + \text{h.c.} \quad (\text{A3})$$

The non-oscillatory part of the 2nd order term in the Weyl square is

$$\delta C^2 \simeq \begin{cases} \frac{324|C_1|^2 \eta_*^3}{M_p^2 a_*^6 \eta^6} & , \text{ large scales} \\ \left(\bar{C}_1 \bar{C}_2^* e^{i\frac{k_L \eta^2}{\eta_*}} + \text{h.c.} \right) \frac{64k_L^6 \eta^2}{M_p^2 a_*^6 k_T^4 \eta_*^5} & , \text{ short scales} \end{cases} . \quad (\text{A4})$$

This behavior is confirmed by the fully numerical solutions shown in the right panel of Figure 6. It is interesting to compare the contribution of the H_\times mode and that of the H_+ mode. In the large scale regime only the contribution of the H_\times mode grows with respect to the background. This is consistent with the amplification of this polarization in the Kasner era that we have found in Section IV. In the small scales regime, the contribution of both modes is instead growing with respect to the background. Although the two modes evolve identically in this regime (since they satisfy the same asymptotic equation), the time evolution of the corresponding δC^2 term is different, since the two modes enter differently in the Weyl tensor.

b. H_+ mode during contraction

Plugging (35) into (40) we have the early / late time expansions

$$\omega_+^2 \simeq \begin{cases} k_L^2 \left(\frac{-\eta}{-\eta_*} \right)^2 & , \text{ short scales} \\ \frac{1}{4(-\eta)^2} + k_T^2 \frac{-\eta_*}{-\eta} & , \text{ large scales} \end{cases} . \quad (\text{A5})$$

The similarities and differences between the H_+ mode in the expanding and contracting cases are identical to those discussed in the previous Subsection for the H_\times mode. We have the asymptotic solutions

$$H_+ \simeq \begin{cases} \frac{C_1}{\sqrt{-\eta}} e^{i \frac{k_L (-\eta)^2}{2(-\eta_*)}} + \frac{C_2}{\sqrt{-\eta}} e^{-i \frac{k_L (-\eta)^2}{2(-\eta_*)}} & , \text{ short scales} \\ \bar{C}_1 \sqrt{-\eta} J_0 \left(2 k_T \sqrt{(-\eta_*) (-\eta)} \right) + \bar{C}_2 \sqrt{-\eta} Y_0 \left(2 k_T \sqrt{(-\eta_*) (-\eta)} \right) & , \text{ large scales} \end{cases} . \quad (\text{A6})$$

This leads to the following asymptotic evolution for the linear term in the square of the Weyl tensor

$$C \delta C \simeq e^{-i k_L x - i k_T y} \times \left\{ \begin{array}{l} \left(C_1 e^{\frac{i k_L (-\eta)^2}{2(-\eta_*)}} + C_2 e^{-\frac{i k_L (-\eta)^2}{2(-\eta_*)}} \right) \frac{12 \sqrt{2} k_T^2 (-\eta_*)^{7/2}}{M_p a_*^5 (-\eta)^6} & , \text{ short scales} \\ - \left[3 \pi \bar{C}_1 + 6 \bar{C}_2 \left(\ln \left(k_T \sqrt{(-\eta_*) (-\eta)} \right) + \gamma - \frac{2}{3} \right) \right] \\ \quad \times \frac{12 \sqrt{2} (-\eta_*)^{5/2}}{\pi M_p a_*^5 (-\eta)^6} & , \text{ large scales} \end{array} \right\} + \text{h.c.} \quad (\text{A7})$$

and for the non-oscillatory part in the quadratic term of the square of the Weyl tensor

$$\delta C^2 \simeq \begin{cases} \left(C_1 C_2^* e^{\frac{i k_L \eta^2}{\eta_*}} + \text{h.c.} \right) \frac{64 k_L^6 (-\eta)^2}{M_p^2 a_*^6 k_T^4 (-\eta_*)^5} & , \text{ short scales} \\ \frac{-120 |\bar{C}_2|^2 (-\eta_*)^2}{M_p^2 \pi^2 a_*^6 k_T^2 (-\eta)^7} & , \text{ large scales} \end{cases} . \quad (\text{A8})$$

This behavior is confirmed by the fully numerical evolutions shown in the right panel of Figure 7.

APPENDIX B: INSTABILITY OF KASNER SOLUTION: KL VS GW

Our analysis of the squared Weyl invariant shows that the Kasner background is unstable due to the amplification of the GW perturbations H_+ and H_\times . This is manifest by the growth of $\delta C/C$ and $\delta C^2/C^2$ summarized in table I. For the contracting background we found that the contribution to $\delta C^2/C^2$ of the polarizations H_+ and H_\times grow, respectively, as $|t|^{-2/3}$ and as $|t|^{-2}$ asymptotically close to the singularity. Conversely, in the expanding case, the Weyl invariant is regular near the singularity. The reason for this discrepancy is that, in the expanding case, we disregarded the Neumann term Y_0 (for H_+) and Y_3 (for H_\times) in the solutions of the evolution equations (39) for the two modes. However these two modes are generally excited as the contracting Kasner background solution approaches the singularity.

The purpose of this Appendix is to show explicitly that this instability is not inconsistent with the lore of alternation of Kasner exponents [29]. On the contrary, the instability in the contracting case was pointed out already in [28], where it was shown that the Kasner background is stable provided one physical condition is imposed. As we now show, the physical condition imposed by [28] precisely eliminates the unstable Y_0 and Y_3 solutions.

We start by quoting the results of [28] where the authors considered a perturbed vacuum Kasner solution in synchronous gauge and did a stability analysis near the singularity. In the main text, we describe the contracting Kasner background using negative time. In [28], instead, positive time was used, and the approach to the singularity was studied in the $t \rightarrow 0^+$ limit. In this Appendix, we adopt the time convention of [28]. Moreover, we specify the analysis of [28] to the axisymmetric $p_1 = -1/3$, $p_2 = p_3 = 2/3$ case. For this choice, the solution obtained in [28] for $t \rightarrow 0^+$ reads

$$\begin{aligned}
 h_1^1 &= A_1 + B_1 \ln t \quad , \quad h_2^2 = A_2 + B_2 \ln t \quad , \quad h_3^3 = A_3 + B_3 \ln t \quad , \\
 h_{12} &= t^{-2/3} \left[C_{12} - \frac{9}{32} k_3 (k_2 C_{13} - k_3 C_{12}) t^{2/3} \right] + t^{4/3} C_{21} \quad , \\
 h_{13} &= t^{-2/3} \left[C_{13} - \frac{9}{32} k_2 (k_3 C_{12} - k_2 C_{13}) t^{2/3} \right] + t^{4/3} C_{31} \quad , \\
 h_{23} &= t^{4/3} (C_{23} + C_{32}) \quad ,
 \end{aligned} \tag{B1}$$

with constants A_i, B_i, C_{ij} satisfying the constraints

$$\begin{aligned}
B_1 + B_2 + B_3 &= -\frac{1}{3}B_1 + \frac{2}{3}(B_2 + B_3) = 0, \\
k_1(B_1 - A_2 - A_3) + 2(k_2 C_{21} + k_3 C_{31}) &= 0, \\
k_2(B_2 + A_1) - 2k_1 C_{12} &= 0, \\
k_3(B_3 + A_1) - 2k_1 C_{13} &= 0.
\end{aligned} \tag{B2}$$

As a result of the synchronous gauge, the solutions (B1) still have freedom due to gauge artifacts; the corresponding gauge contributions to the perturbations are given in eqs (F3) of [28]. Using this freedom, the Authors of [28] set $C_{12} = C_{31} = C_{23} + C_{32} = 0$.⁸ After this gauge fixing, one sees that the mode h_{13} diverges at the singularity. For this reason, ref. [28] concluded that the Kasner background is stable only provided the condition $C_{13} = 0$ is imposed. We stress that setting C_{13} is not a gauge choice, but rather the suppression of a physical degree of freedom. This physical constraint, along with the relations (B2), implies that $B_2 = 0$.

We now turn back to our analysis. For $t \rightarrow 0^+$, eqs. (39) admit the solutions

$$\begin{aligned}
H_+ &= t^{1/3} [D_1 J_0(3 k_T t^{1/3}) + D_2 Y_0(3 k_T t^{1/3})], \\
H_\times &= t^{1/3} [E_1 J_3(3 k_T t^{1/3}) + E_2 Y_3(3 k_T t^{1/3})].
\end{aligned} \tag{B3}$$

The modes J_0 and J_3 are regular at the singularity, whereas Y_0 and Y_3 diverge, thus resulting in the instability. We now show that the conditions $C_{12} = C_{13} = B_2$ in [28] correspond to having $D_2 = E_2 = 0$ in our case. To do such a comparison, we need to change from the gauge chosen in the main text to the synchronous gauge adopted in [28]. We do so through a general infinitesimal transformation $x^\mu \rightarrow x^\mu + \xi^\mu$, with $\xi^\mu = (\xi^0, \partial_1 \xi^1, \partial^i \xi + \xi^i)$ where ξ^i is a transverse 2d vector. From the transformed metric $\delta g_{\mu\nu} \rightarrow \delta g_{\mu\nu} - \mathcal{L}_\xi g_{\mu\nu}^{(0)}$, we find that

⁸ They are in fact setting $C_{23} = 0$ in the general case. However, the time dependences of both terms in h_{23} are the equal to each other for the axisymmetric $p_2 = p_3$ case; therefore, in this case, the removal of the gauge artifact corresponds to $C_{23} + C_{32} = 0$.

the parameters ξ^μ which take our gauge to the synchronous coordinates are

$$\begin{aligned}
\xi^0 &= \frac{1}{a_{\text{av}}} \int^t dt' \Phi(t') + \frac{1}{a_{\text{av}}} f^0, \\
\xi^1 &= \int^t dt' \frac{\chi(t')}{a(t')} + \int^t \frac{dt'}{a^2(t')} \int^{t'} dt'' \Phi(t'') + f^0 \int^t \frac{dt'}{a^2(t')} + f^1, \\
\xi &= \int^t dt' \frac{B(t')}{b(t')} + \int^t \frac{dt'}{b^2(t')} \int^{t'} dt'' \Phi(t'') + f^0 \int^t \frac{dt'}{b^2(t')} + f, \\
\xi^i &= \int^t dt' \frac{B_i(t')}{b(t')} + f^i,
\end{aligned} \tag{B4}$$

where f^0, f^1, f, f^i are integration constants and $k_i f^i = 0$. The perturbations Φ, χ, B and B_i are the modes in the decomposition given in the main text. Using their relations to the canonical modes H_+ and H_\times , along with the early time solutions (B3), we calculate the metric perturbations in synchronous gauge. The relevant components for the present discussion are

$$\begin{aligned}
h_{12} &= -\frac{16 i \sqrt{2} k_3}{27 \pi k_T^4 M_p} E_2 \left(t^{-2/3} + \frac{9}{8} k_T^2 + \frac{81}{64} k_T^4 t^{2/3} \right) - \frac{12}{5} f^0 k_1 k_2 t + k_1 k_2 f^1 t^{-2/3} + \mathcal{O}(t^{4/3}), \\
h_{13} &= \frac{16 i \sqrt{2} k_2}{27 \pi k_T^4 M_p} E_2 \left(t^{-2/3} + \frac{9}{8} k_T^2 + \frac{81}{64} k_T^4 t^{2/3} \right) - \frac{12}{5} f^0 k_1 k_3 t + k_1 k_3 f^1 t^{-2/3} + \mathcal{O}(t^{4/3}), \\
h_2^2 &= -\frac{\sqrt{2}}{3 \pi M_p} \left[3 \pi D_1 + 2 (3 \gamma - 2) D_2 + 6 D_2 \ln \left(\frac{3 k_T}{2} \right) \right] \\
&\quad + \frac{2 \sqrt{2}}{27 \pi k_T^5 M_p} \left[-32 i k_1 k_2 \frac{k_3}{k_T} E_2 - 9 D_2 k_T^3 (k_3^2 - k_2^2) \right] \ln t \\
&\quad - 2 f_0 \left(3 k_2^2 t^{-1/3} + \frac{2}{3 t} \right) + 2 k_2 (i f_2 + k_2 f) + \mathcal{O}(t^{2/3}).
\end{aligned} \tag{B5}$$

In eqs (B1), setting $C_{12} = 0$ (gauge choice) and $C_{13} = 0$ (physical choice) eliminates the terms up to $\mathcal{O}(t^{4/3})$ in h_{12} and h_{13} . On the other hand, from our solution (B5), we see that these terms in h_{1i} vanish only if $E_2 = 0$. Furthermore, the choice $C_{12} = C_{13} = 0$ implies that $B_2 = 0$, now eliminating the log term in h_2^2 , which corresponds to $D_2 = 0$ in our solutions. In other words, the stability conditions derived in [28] correspond to removing the Neumann functions in the early time solutions (B3) of both H_+ and H_\times .

APPENDIX C: EXPLICIT COMPUTATION OF $C_{\ell\ell'mm'}$

Here, we prove the relation (50) of the main text. This expression gives the C_ℓ coefficients of the temperature anisotropies in terms of the value of the power spectrum of GW at the end

of inflation. Therefore, this computation is performed in an isotropic universe. The effects of the anisotropic stage are encoded in the power spectra that, on large scales, depend also on the orientation of the modes.

We start by decomposing the temperature perturbations in direction $\hat{\mathbf{p}}$ measured by an observer at \mathbf{x}_0 and at conformal time η_0 , into spherical harmonics

$$\frac{\delta T}{T}(\hat{\mathbf{p}}) = \sum_{\ell, m} a_{\ell m} Y_{\ell m}(\hat{\mathbf{p}}). \quad (\text{C1})$$

Assuming that the perturbations are Gaussian, their statistics are completely specified by the second order correlations, which can be written by inverting (C1)

$$C_{\ell\ell'mm'} \equiv \langle a_{\ell m} a_{\ell' m'}^* \rangle = \int d\Omega_{\hat{\mathbf{p}}} d\Omega_{\hat{\mathbf{p}'}} \left\langle \frac{\delta T}{T}(\hat{\mathbf{p}}) \frac{\delta T}{T}(\hat{\mathbf{p}'}) \right\rangle Y_{\ell m}^*(\hat{\mathbf{p}}) Y_{\ell' m'}(\hat{\mathbf{p}'}). \quad (\text{C2})$$

Assuming instantaneous recombination, we can use the well-known solution to the first order Boltzmann equation for gravity waves:

$$\frac{\delta T}{T}(\hat{\mathbf{p}}) = -\frac{1}{2} \int_{\eta_{\text{LSS}}}^{\eta_0} d\eta \frac{\partial h_{ij}}{\partial \eta} \hat{p}^i \hat{p}^j, \quad (\text{C3})$$

where $h_{ij} \equiv \delta g_{ij}/a^2$. We expand the gravitational perturbations in terms of plane waves as

$$h_{ij}(\mathbf{x}, \eta_0) = \sum_{\lambda=+, \times} \int \frac{d^3 k}{(2\pi)^{3/2}} e^{i\mathbf{k}\cdot\mathbf{x}} \epsilon_{ij}^{(\lambda)}(\mathbf{k}) h^{(\lambda)}(\mathbf{k}, \eta) a_{\mathbf{k}}^{(\lambda)} \quad (\text{C4})$$

where (λ) designates the two polarizations (+) and (\times), $\epsilon_{ij}^{(\lambda)}(\mathbf{k})$ is the normalized polarization tensor satisfying $\epsilon_{ij}^{(\lambda)}(\mathbf{k}) \epsilon_{i'j'}^{(\lambda')}(\mathbf{k}) = \delta_{(\lambda)(\lambda')}$, and $a_{\mathbf{k}}^{(\lambda)}$ are Gaussian random variables with unit dispersion, ie. $\langle a_{\mathbf{k}}^{(\lambda)}, a_{\mathbf{k}'}^{*(\lambda')} \rangle = \delta^{(3)}(\mathbf{k} - \mathbf{k}') \delta_{(\lambda)(\lambda')}$. Using the solution (C3) along with the decomposition (C4) in the expression (C2), we get

$$\begin{aligned} C_{\ell\ell'mm'} &= \frac{1}{4} \sum_{\lambda} \int \frac{d^3 k}{(2\pi)^3} \int d\Omega_{\hat{\mathbf{p}}} d\Omega_{\hat{\mathbf{p}'}} Y_{\ell m}^*(\hat{\mathbf{p}}) Y_{\ell' m'}(\hat{\mathbf{p}'}) \\ &\quad \times \left[\int d\eta \left(\frac{\partial}{\partial \eta} h^{(\lambda)}(\mathbf{k}, \eta) \right) e^{i\mathbf{k}\cdot\hat{\mathbf{p}}(\eta-\eta_0)} \epsilon_{ij}^{(\lambda)}(\mathbf{k}) \hat{p}^i \hat{p}^j \right] \\ &\quad \times \left[\int d\tilde{\eta} \left(\frac{\partial}{\partial \tilde{\eta}} h^{(\lambda)}(\mathbf{k}, \tilde{\eta}) \right) e^{i\mathbf{k}\cdot\hat{\mathbf{p}}'(\tilde{\eta}-\eta_0)} \epsilon_{ab}^{(\lambda)}(\mathbf{k}) \hat{p}'^a \hat{p}'^b \right]^*, \end{aligned} \quad (\text{C5})$$

where we noted that $\mathbf{x} = \mathbf{x}_0 + \hat{\mathbf{p}}(\eta - \eta_0)$ describes the geodesics of the photons with direction $\hat{\mathbf{p}}$, observed at (\mathbf{x}_0, η_0) .

The contraction $\epsilon_{ij}^{(\lambda)}(\mathbf{k}) \hat{p}^i \hat{p}^j$ can be calculated in terms of the angles of $\hat{\mathbf{p}}$ defined with respect to a coordinate system with a z -axis coinciding with $\hat{\mathbf{k}}$, as [26]

$$\epsilon_{ij}^{(\lambda)}(\mathbf{k}) \hat{p}^i \hat{p}^j = \left[\delta_{(+)}^{(\lambda)} \cos(2\phi_{\hat{p}_k}) + \delta_{(\times)}^{(\lambda)} \sin(2\phi_{\hat{p}_k}) \right] \sin^2 \theta_{\hat{p}_k}. \quad (\text{C6})$$

To take the angular integral over $d\Omega_{\hat{p}}$ ($d\Omega_{\hat{p}'}$), we first rotate the spherical harmonics to the angular basis $\hat{p}_{\hat{k}}$ ($\hat{p}'_{\hat{k}}$) with

$$Y_{\ell m}(\hat{\mathbf{p}}) = \sum_M D_{mM}^{\ell*}(\hat{\mathbf{k}}) Y_{\ell M}(\hat{\mathbf{p}}_{\hat{\mathbf{k}}}), \quad (\text{C7})$$

where $D_{mM}^{\ell*}$ are the Wigner coefficients satisfying $\sum_M D_{Mm}^{\ell} D_{Mm'}^{\ell*} = \delta_{mm'}$. Finally, the angular integrals can be evaluated as [26]

$$\begin{aligned} \int d\Omega_{\hat{p}_{\hat{k}}} Y_{\ell m}^*(\hat{\mathbf{p}}_{\hat{\mathbf{k}}}) e^{i\mathbf{k}\cdot\hat{\mathbf{p}}(\eta-\eta_0)} \epsilon_{ij}^{(\lambda)}(\mathbf{k}) \hat{p}^i \hat{p}^j &= -(-i)^\ell \pi \sqrt{\frac{(2\ell+1)(\ell+2)!}{2(\ell-2)!} \frac{J_{\ell+1/2}[k(\eta_0-\eta)]}{[k(\eta_0-\eta)]^{5/2}}} \\ &\times \left[\left(\delta_{(+)}^{(\lambda)} - i \delta_{(\times)}^{(\lambda)} \right) \delta_{M,2} + \left(\delta_{(+)}^{(\lambda)} + i \delta_{(\times)}^{(\lambda)} \right) \delta_{M,-2} \right]. \end{aligned} \quad (\text{C8})$$

Ignoring the effect on the (small scale) modes which enter the horizon during the radiation dominated era, the solutions for the gravity waves during matter domination can be written in terms of the primordial one as [25], [27]

$$h^{(\lambda)}(\mathbf{k}, \eta) = 3 \sqrt{\frac{\pi}{2}} \frac{J_{3/2}(k\eta)}{(k\eta)^{3/2}} h^{(\lambda)}(\mathbf{k}, 0). \quad (\text{C9})$$

Using the integral (C8) along with the above solution yields

$$\begin{aligned} C_{\ell\ell'mm'} &= \sum_{\lambda, M, M'} (-i)^{\ell-\ell'} \frac{9\pi^3}{16} \sqrt{\frac{(2\ell+1)(2\ell'+1)(\ell+2)! (\ell'+2)!}{(\ell-2)! (\ell'-2)!}} \\ &\times \left[(\delta_{M,2} \delta_{M',2} + \delta_{M,-2} \delta_{M',-2}) (\delta_{\lambda}^+ + \delta_{\lambda}^{\times}) + (\delta_{M,-2} \delta_{M',2} + \delta_{M,2} \delta_{M',-2}) (\delta_{\lambda}^+ - \delta_{\lambda}^{\times}) \right] \\ &\times \int_0^\infty \frac{dk}{k} I_\ell^2(k\eta_0) \int_{-1}^{+1} \frac{d\xi}{2} \int_0^{2\pi} \frac{d\phi_k}{2\pi} D_{mM}^{\ell}(\hat{\mathbf{k}}) D_{m'M'}^{\ell'*}(\hat{\mathbf{k}}) P_{H_\lambda}(\mathbf{k}), \end{aligned} \quad (\text{C10})$$

where $\xi \equiv \cos\theta_k$, the power spectrum is defined through

$$P_{H_\lambda}(\mathbf{k}) = \frac{k^3 |h^{(\lambda)}(\mathbf{k}, 0)|^2}{2\pi^2}, \quad (\text{C11})$$

which coincides with the definitions given in the main text, cf. eqs. (29) and (33) once the universe has isotropized. Finally, the time integral is

$$I_\ell(k\eta_0) \equiv \int_{k\eta_{\text{LSS}}}^{k\eta_0} dy \frac{J_{5/2}(y)}{y^{3/2}} \frac{J_{\ell+1/2}(k\eta_0-y)}{(k\eta_0-y)^{5/2}}. \quad (\text{C12})$$

To be able to compare with observations, we average the diagonal ($\ell = \ell'$, $m = m'$) part of the correlator over all m and obtain

$$\begin{aligned} C_\ell &= \frac{1}{2\ell+1} \sum_m C_{\ell\ell mm} \\ &= \frac{9\pi^3}{8} \frac{(\ell+2)!}{(\ell-2)!} \int_0^\infty \frac{d(k\eta_0)}{(k\eta_0)} I_\ell^2(k\eta_0) \int_{-1}^{+1} \frac{d\xi}{2} \int_0^{2\pi} \frac{d\phi_k}{2\pi} [P_{H_+}(\mathbf{k}) + P_{H_\times}(\mathbf{k})], \end{aligned} \quad (\text{C13})$$

The final result (C13) is valid for any model of pre-inflation which results in an anisotropic primordial tensor power spectrum.

For standard (isotropic) inflation, the power spectrum is the same for both polarizations and we recover the standard result [25].

-
- [1] G. Hinshaw *et al.* [WMAP Collaboration], arXiv:0803.0732 [astro-ph].
 - [2] [Planck Collaboration], arXiv:astro-ph/0604069.
 - [3] C. E. North *et al.*, arXiv:0805.3690 [astro-ph].
 - [4] P. Oxley *et al.*, Proc. SPIE Int. Soc. Opt. Eng. **5543**, 320 (2004) [arXiv:astro-ph/0501111].
 - [5] C. J. MacTavish *et al.*, arXiv:0710.0375 [astro-ph].
 - [6] J. Bock *et al.*, arXiv:0805.4207 [astro-ph].
 - [7] E. S. Phinney *et al.* (The Big Bang Observer), NASA Mission Concept Study (2003); <http://universe.nasa.gov/program/vision.html>
 - [8] N. Seto, S. Kawamura and T. Nakamura, Phys. Rev. Lett. **87**, 221103 (2001) [arXiv:astro-ph/0108011].
 - [9] D. S. Goldwirth and T. Piran, Phys. Rept. **214**, 223 (1992).
 - [10] A. Starobinsky, Sov. Phys. Lett. **37** (1983) 67; G. Steigman and M. S. Turner, Phys. Lett. B **128**, 295 (1983); T. Rothman and M. S. Madsen, Phys. Lett. B **159**, 256 (1985).
 - [11] A. E. Gumrukcuoglu, C. R. Contaldi and M. Peloso, Proceedings of the Eleventh Marcel Grossmann Meeting on General Relativity, ed. H. Kleinert, R.T. Jantzen & R. Ruffini, World Scientific, 2007, ArXiv Astrophysics e-prints, arXiv:astro-ph/0608405.
 - [12] T. S. Pereira, C. Pitrou and J. P. Uzan, JCAP **0709**, 006 (2007) [arXiv:0707.0736 [astro-ph]].
 - [13] A. E. Gumrukcuoglu, C. R. Contaldi and M. Peloso, JCAP **0711**, 005 (2007) [arXiv:0707.4179 [astro-ph]].
 - [14] C. Pitrou, T. S. Pereira and J. P. Uzan, JCAP **0804**, 004 (2008) [arXiv:0801.3596 [astro-ph]].
 - [15] G. Nicholson and C. R. Contaldi, JCAP **0801**, 002 (2008) [arXiv:astro-ph/0701783].
 - [16] A. R. Pullen and M. Kamionkowski, Phys. Rev. D **76**, 103529 (2007) [arXiv:0709.1144 [astro-ph]].
 - [17] S. Kachru, R. Kallosh, A. Linde, J. M. Maldacena, L. McAllister and S. P. Trivedi, JCAP **0310**, 013 (2003) [arXiv:hep-th/0308055].

- [18] J. P. Conlon and F. Quevedo, JHEP **0601**, 146 (2006) J. R. Bond, L. Kofman, S. Prokushkin and P. M. Vaudrevange, Phys. Rev. D **75**, 123511 (2007) [arXiv:hep-th/0612197]. [arXiv:hep-th/0509012];
- [19] V. F. Mukhanov, JETP Lett. **41**, 493 (1985) [Pisma Zh. Eksp. Teor. Fiz. **41**, 402 (1985)]; M. Sasaki, Prog. Theor. Phys. **76**, 1036 (1986).
- [20] A. Riotto, arXiv:hep-ph/0210162.
- [21] D. Garfinkle, Phys. Rev. Lett. **93**, 161101 (2004) [arXiv:gr-qc/0312117].
- [22] A. R. Liddle and D. H. Lyth, *Cambridge, UK: Univ. Pr. (2000) 400 p*
- [23] D. I. Podolsky, G. N. Felder, L. Kofman and M. Peloso, Phys. Rev. D **73**, 023501 (2006) [arXiv:hep-ph/0507096].
- [24] G. Hinshaw *et al.* [WMAP Collaboration], Astrophys. J. Suppl. **170**, 288 (2007) [arXiv:astro-ph/0603451].
- [25] A. A. Starobinsky, Sov. Astron. Lett. **11**, 133 (1985).
- [26] M. J. White, Phys. Rev. D **46**, 4198 (1992) [arXiv:hep-ph/9207239].
- [27] M. S. Turner, M. J. White and J. E. Lidsey, Phys. Rev. D **48**, 4613 (1993) [arXiv:astro-ph/9306029].
- [28] E. M. Lifshitz and I. M. Khalatnikov, Adv. Phys. **12**, 185 (1963).
- [29] V. A. Belinsky, I. M. Khalatnikov and E. M. Lifshitz, Adv. Phys. **19**, 525 (1970).
- [30] V. Belinskii, I. Khalatnikov and E. Lifshitz, Adv. Phys. **31** (1982) 639.
- [31] T. Damour, M. Henneaux and H. Nicolai, Class. Quant. Grav. **20**, R145 (2003) [arXiv:hep-th/0212256].
- [32] T. Damour and S. de Buyl, Phys. Rev. D **77**, 043520 (2008) [arXiv:0710.5692 [gr-qc]].
- [33] L. Andersson, H. van Elst, W. C. Lim and C. Uggla, Phys. Rev. Lett. **94**, 051101 (2005) [arXiv:gr-qc/0402051].
- [34] C. Uggla, H. van Elst, J. Wainwright and G. F. R. Ellis, Phys. Rev. D **68**, 103502 (2003) [arXiv:gr-qc/0304002].
- [35] J. Wainwright, in “Dynamical Systems in Cosmology”, pp. 123-155, eds J. Wainwright and J. Ellis, Cambridge U Press 1997.
- [36] T. Damour and M. Henneaux, Phys. Rev. Lett. **86**, 4749 (2001) [arXiv:hep-th/0012172].
- [37] B. Freivogel, M. Kleban, M. Rodriguez Martinez and L. Susskind, JHEP **0603**, 039 (2006) [arXiv:hep-th/0505232].